



Dissimilar friction-stir welding of aluminum and polymer: a review

Meysam Haghshenas¹ · Farzad Khodabakhshi²

Received: 1 March 2019 / Accepted: 16 May 2019 / Published online: 31 May 2019
© Springer-Verlag London Ltd., part of Springer Nature 2019

Abstract

Newly, linear friction-stir welding (FSW) was introduced and implemented as a very effective and emerging solid-state technology for the dissimilar joining of metals and non-metals such as polymers. This kind of joint design is very interesting for structural applications especially in the case of the automotive industry. In this regard, several combinations of materials in terms of metals (mainly focused on aluminum) and polymers (mostly thermoplastic compounds) were assessed in two joint designs as butt and lap in terms of processing parameters optimization, microstructural features, interfacial bonding, and mechanical behavior. This systematic review article deals with overviewing the previous studies on this specific object to categorize the existing knowledge and open some new windows for future developments.

Keywords Friction-stir welding (FSW) · Dissimilar joining · Metal · Polymer · Mechanical bonding

1 Introduction

Global trends push the transportation sectors to make lighter, safer, greener, and finally less expensive vehicles [1]. To this end, non-metals (i.e., polymers, polymer-based composites) as well as non-metal/metal bi-material structures can be potentially employed in various products to save the associated density of the final product(s) [2]. Novel thermoplastic materials are employed largely in the structural and engineering applications, like automotive and aerospace sectors, thanks to their improved specific strength as well as low cost [3]. Polyethylene is one of the most commonly used thermoplastics employed in a vast variety of manufacturing applications thanks to the easy manufacturing process in various shapes [4]. Although there exist lack of restrictions and great fabrication feasibility when utilizing the thermoplastics [5], the assembly of intricate and complex-in-shape components demands the joining to the different various materials including metals and non-metals [4, 6].

When employing hybrid technology by marrying metals and non-metals, two completely different materials are integrated into an individual part and/or assembly [7, 8]. To more effectively fulfill the customer requirements one can get benefited from “hybrid” approach to gain advantages of both partners (i.e., low density from polymeric and high strength from metallic materials) [9]. The leading case of a booming integration of metals and polymers in manufacturing a hybrid structure goes back to late 1996 when the front end of the Audi A6 was manufactured out of a metallic partner (steel sheet) with a non-metallic counterpart (elastomer-modified polyamide PA6-GF30) [9]. The winning point of a hybrid structure is that the end properties cannot be found in the individual partners and the hybrid component can get the best use of the base materials [10]. Currently, automakers are paying more and more attention to hybrid components as a promising alternative to all-metallic structures for various modules of the vehicle [7]. Some automobile-related examples, where a hybrid structure is employed, include instrument-panel and bumper cross-beams, door modules, and tailgates [11].

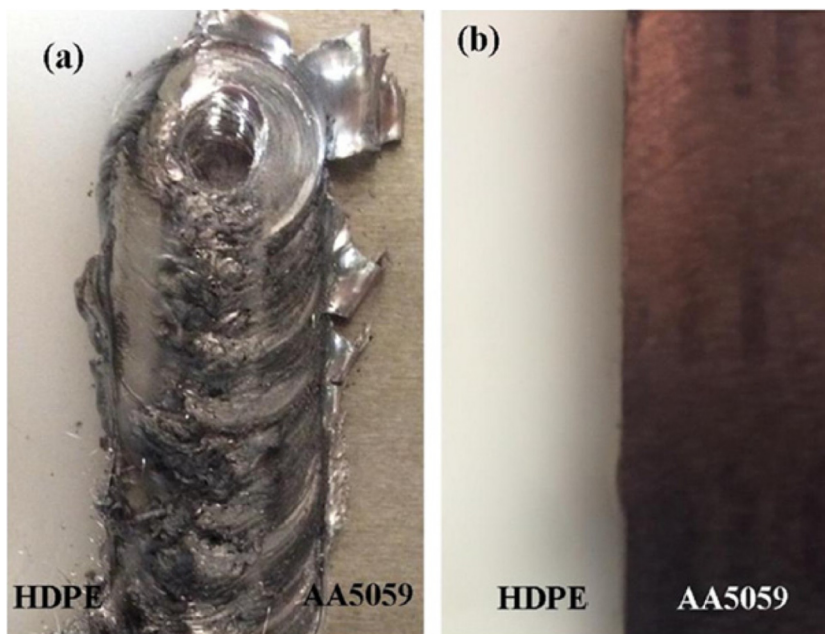
The design of such large complex engineering structures composed of a combination of dissimilar materials requires advanced and alternative joining technologies [3]. The main joining methods for polymer and polymeric composites are mechanical fastening, adhesive bonding, and welding [9]. Plastic welding processes can be divided into two main groups: processes involving mechanical movement to produce heat (ultrasonic welding, friction welding, vibration welding) and processes involving external heating (hot plate

✉ Farzad Khodabakhshi
fkhodabakhshi@ut.ac.ir

¹ Department of Mechanical Engineering, University of North Dakota, Grand Forks, ND, USA

² School of Metallurgical and Materials Engineering, College of Engineering, University of Tehran, P.O. Box: 11155-4563, Tehran, Iran

Fig. 1 Dissimilar friction-stir welds between AA5059 and HDPE. (a) Front surface appearance. (b) Black view [42]



welding, hot gas welding, resistive, and implant welding) [12]. Welding techniques for plastics are nowadays consolidated processes in several industrial areas [13, 14]. However, their applications are still limited to some polymer grades and joint configurations [15]. Therefore, polymer-metal structures are more difficult to join by traditional joining methods, mostly due to their dissimilarity in physical-chemical features [6, 16]. Technological limitations, such as the requirements of extensive surface treatments and long curing times in the case of adhesive bonding as well as the stress concentration and weight penalty related to mechanical fastening, have motivated the recent investigations on new joining techniques [17].

Amancio et al. [6] ordered diverse joining advances for polymer-metal hybrid structures, going from progressively ordinary glue holding and mechanical affixing to new welding-based innovations, for example, ultrasonic welding [18] and enlistment welding [19]. Abibe et al. [20] explored the mechanical and disappointment conduct of polymer-metal joints utilizing infusion securing joining, an innovation dependent on staking and mechanical affixing. The achievability of joining glass-fiber-fortified thermoplastic composites with titanium review 2 utilizing grinding riveting was researched by Bлага et al. [21]. Balle et al. [22] explored the achievability and mechanical properties of ultrasonic spot welding of aluminum/carbon-fiber fortified polymers and upgraded the procedure parameters that accomplished a semi-static ductile shear quality of up to multiple times higher than the weakest base compound [23]. The creators additionally examined the weldability of AA2024/carbon-fiber-fortified polymer utilizing distinctive post-warm medicines, which brought about joints with shear quality as a lot higher [11, 24, 25]. Bergmann and Stambke [16] researched the weldability of steel and polyamide utilizing a laser as the warming source and assessed the impact of process parameters and surface conditions on the mechanical execution of the joints. The

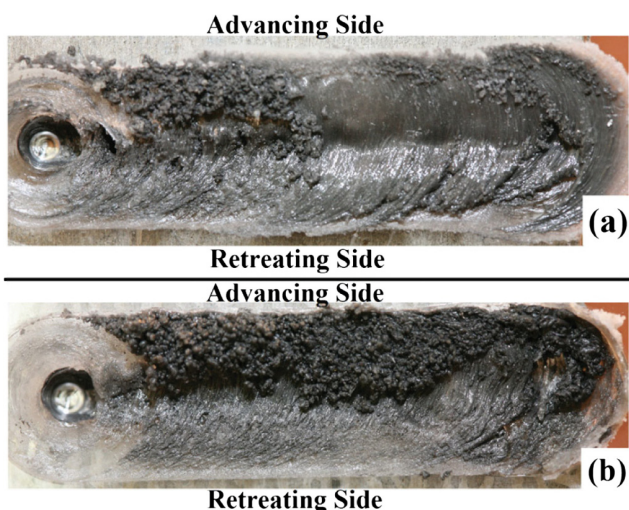
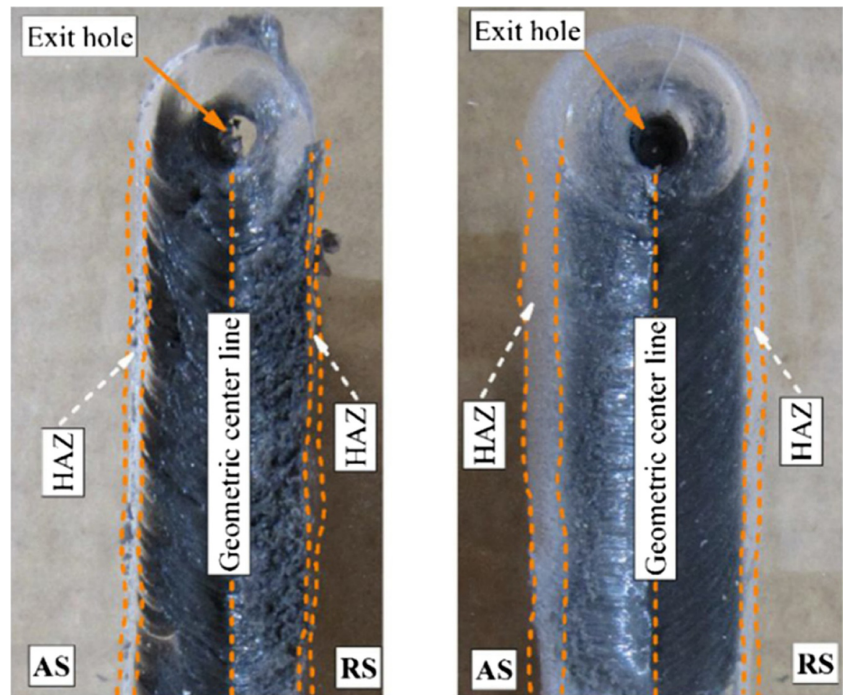


Fig. 2 Top surface dissimilar materials flow for weldments between AA5058 and PMMA at (a) $w = 1250$ rev/min, $v = 50$ mm/min; and (b) $w = 1600$ rev/min, $v = 25$ mm/min [50]

Table 1 The process parameters in FSW of AA5058 and PC [44]

Parameter	Value
Tool rotational speed (rpm)	960, 1200, 1600, 1940
Tool traveling speed (mm/min)	45, 90
Tool tilt angle (degree)	2
Tool plunge depth (mm)	0.3

Fig. 3 The top view surface profile for dissimilar weldment between AA5058 and PC at rotational speeds of (left) 1940 rpm (45 mm/min) and (right) 960 rpm (90 mm/min) [44]

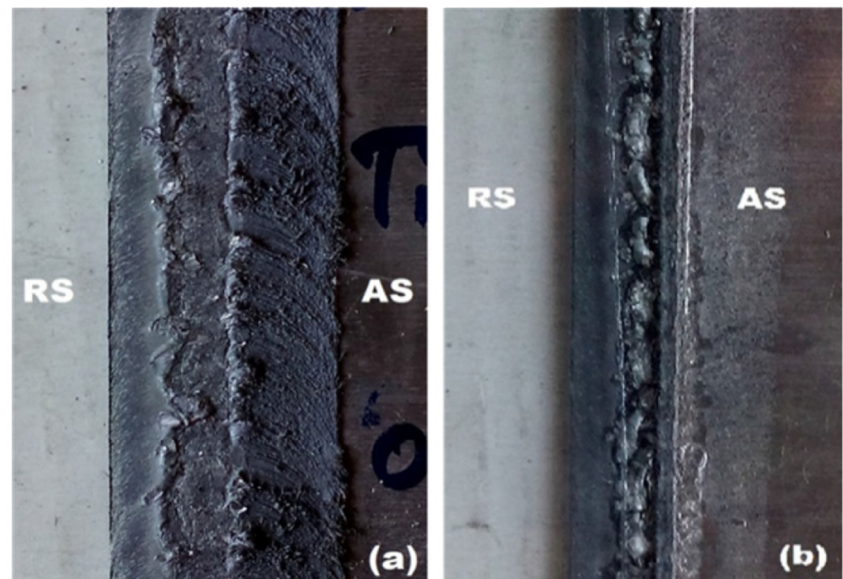


attainability of acceptance welding of steel and Al-Mg composite with carbon-fiber-strengthened thermoplastic and in addition the impact of various metal surface pre-mediations on the joint shear quality were explored and detailed by Mitschang et al. [26].

Steady endeavors on creating enhanced elective joining systems for these crossover structures, for example, the infrared welding, the constrained blended expulsion procedure, and the rubbing mix welding (FSW) [27]. One critical preferred standpoint in contrast with ordinarily utilized mechanical attaching and glues would be the higher get-together rates

and along these lines the decreased gathering costs. FSW is a quickly developing strong state joining process that shows up as a promisingly ecologic weld strategy that empowers to decrease material waste and to evade radiation and unsafe gas emanations generally connected with the combination welding strategies [28, 29]. In FSW, a non-consumable turning instrument appended with a uniquely planned stick is embedded in the butting edges of the plates to be joined [30, 31] and cross along the bond line. Because of collaboration among apparatus and encompassing materials, frictional and disfigurement warm are created [30, 32]. The apparatus revolution and

Fig. 4 Surface morphology of the dissimilar weldment between AA6061 and PC. (a) Front view. (b) Back look [48]



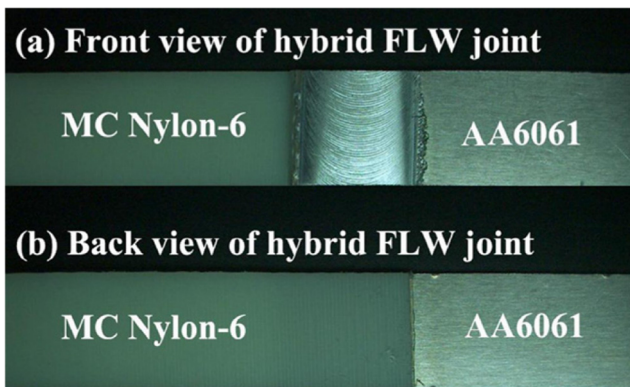


Fig. 5 Front (a) and back (b) views of solid-state hybrid joint between AA6061 and MC Nylon-6 [13]

navigate speed up material spill out of the front to the back of the stick and the welded joint can be created [33, 34].

This emerging solid-state technology was successfully accompanied for the similar and dissimilar joining of various kinds of metals and alloys [35–40]. However, there is some limit activities about dissimilar friction stir welding of metals and non-metals (i.e., polymers) [13, 41–51]. This critical review paper focuses on the impression of the current state of literature in the aspect of dissimilar bonding between various kinds of metals and polymers by the implementation of linear

friction-stir welding technology through the different butt- and lap-joint designs.

2 Characterization of the studied metal/polymer systems

2.1 Dissimilar friction-stir welding

2.1.1 Quality and surface appearance of the dissimilar welded joints

AA5059-HDPE Khodabakhshi et al. [1] studied a solid-state joint (FSW) between a 4-mm-thick aluminum 5059 and a polymeric material (high-density polyethylene (HDPE) sheet). Using a 16-mm-diameter tool and a displacement control milling machine, they tried various spinning and traveling rates of 400–2000 rpm, and 30–200 mm/min, respectively. Figure 1 shows the front and back view of a successful weld between the 5059 aluminum and the HDPE employing a 63 mm/min traveling speed and a 710-rpm tool spinning speed. The front view looks fairly uneven due to the rotating action of the spinning tool, while the back view seems quite smooth and sound.

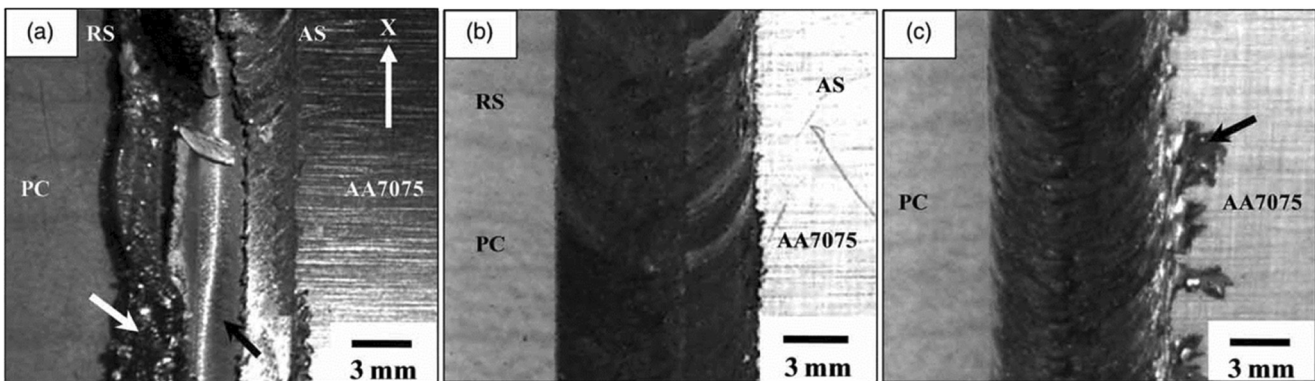
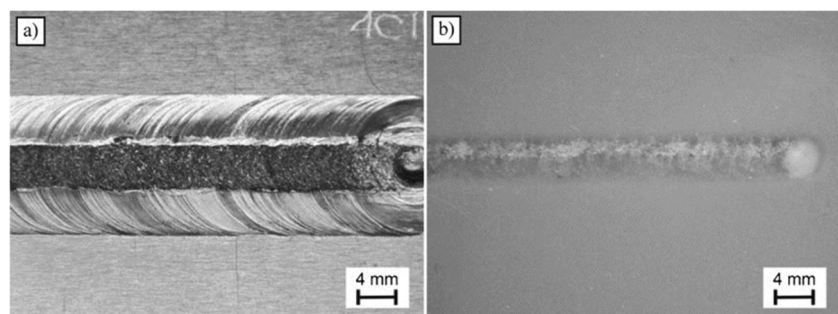


Fig. 6 Surface appearances of the welded joint between AA7075 and PC, utilizing the device with a test of (a) 3-mm length and a measurement of 2 mm with 15° tapered angle, (b) 1 mm length and measurement of 1 mm

with 25° tapered angle, and (c) leftover AA7075 showed up at the welded territory. The progressing and the RS are named AS and RS, separately. X speaks to the instrument navigate bearing [49]

Fig. 7 Friction stirred joint appearances for dissimilar weldment between AA6111 and PPS. (a) Aluminum side. (b) PPS side [41]



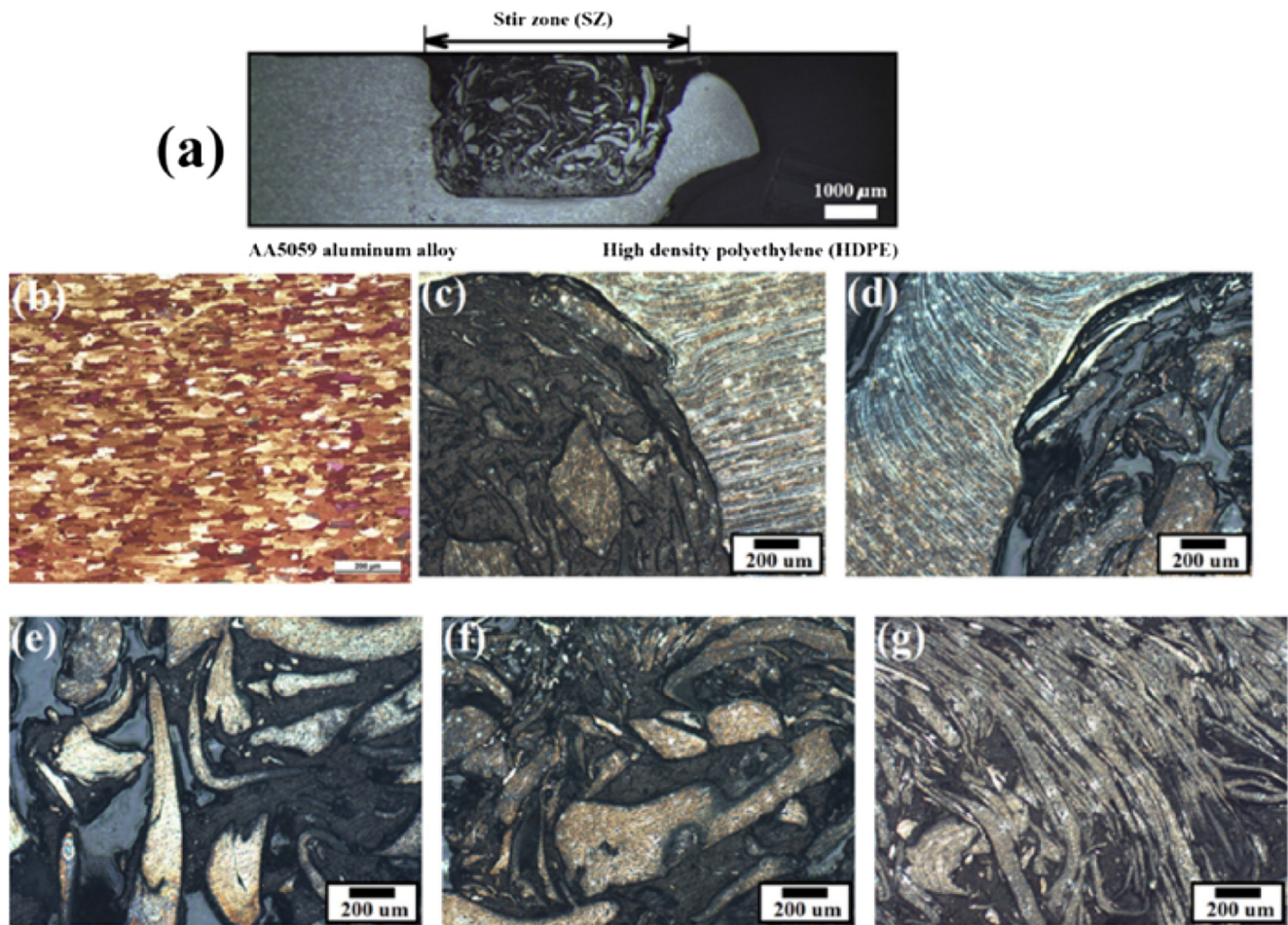


Fig. 8 (a) Macro-image and (b–g) optical micro-image from the SZ of the 5059–HDPE FSW joint [42]

AA5058-PMMA Derazkola et al. [50] assessed the impacts of processing conditions on the features of dissimilar friction-stir-welds between an aluminum alloy (5058) and PMMA polymer. They studied various factors including revolutions per minute, millimeter per minute, tool tilt angle and plunge depth on the surface, materials flow, microstructural features, and mechanical response of the dissimilar FSW joints. They reported a successful dissimilar joint with the uppermost strength of about 45 MPa at a prime processing opening of $w = 1600$ rpm, $v = 25$ mm/min, tool tilt angle of 2° , and plunge depth of 0.2 mm. Figure 2 provides the surface appearance of the joint in the mentioned welding parameters.

AA5058-polycarbonate In a separate study, Derazkola and Elyasi [44] assessed the effect of rpm and mm/min of the friction stir welding (FSW) tool on the lap-joining of a 5058 aluminum alloy and polycarbonate (PC). Table 1 summarizes the parameters they used in their study. They concluded that development of a U-shape macro-lock of aluminum metal toward polymer side is the main microstructural feature in joining the materials.

Figure 3 provides the general shape of the joint line welded at 1940 rpm (45 mm/min) and 960 rpm (90 mm/min).

AA6061-polycarbonate Patel et al. [48] assessed the dissimilar friction stir joining of aluminum alloy (AA6061-T6) and polycarbonate (PC) with the plates of 3-mm thickness. They employed tool rotational speeds and tool traverse speeds as 500–1400 rpm and 40–80 mm/min, respectively. They got the best result employing 500 rpm and 40 mm/min. Figure 4 shows the surface appearance of the welded joint at 500 rpm and 40 mm/min.

AA6061-nylon 6 Liu et al. [13] employed overlap FSW to join sheets of 6061 aluminum alloy, upper sheet, and Nylon 6, lower sheet. They observed no welding distortion and warping thanks to the low peak temperature induced in the process. Figure 5 shows the typical joint samples processed by friction stir lap welding. The semi-circular patterns are clearly visible on the surface of the metallic partner (AA6061) with no visible defects like distortion and warping.

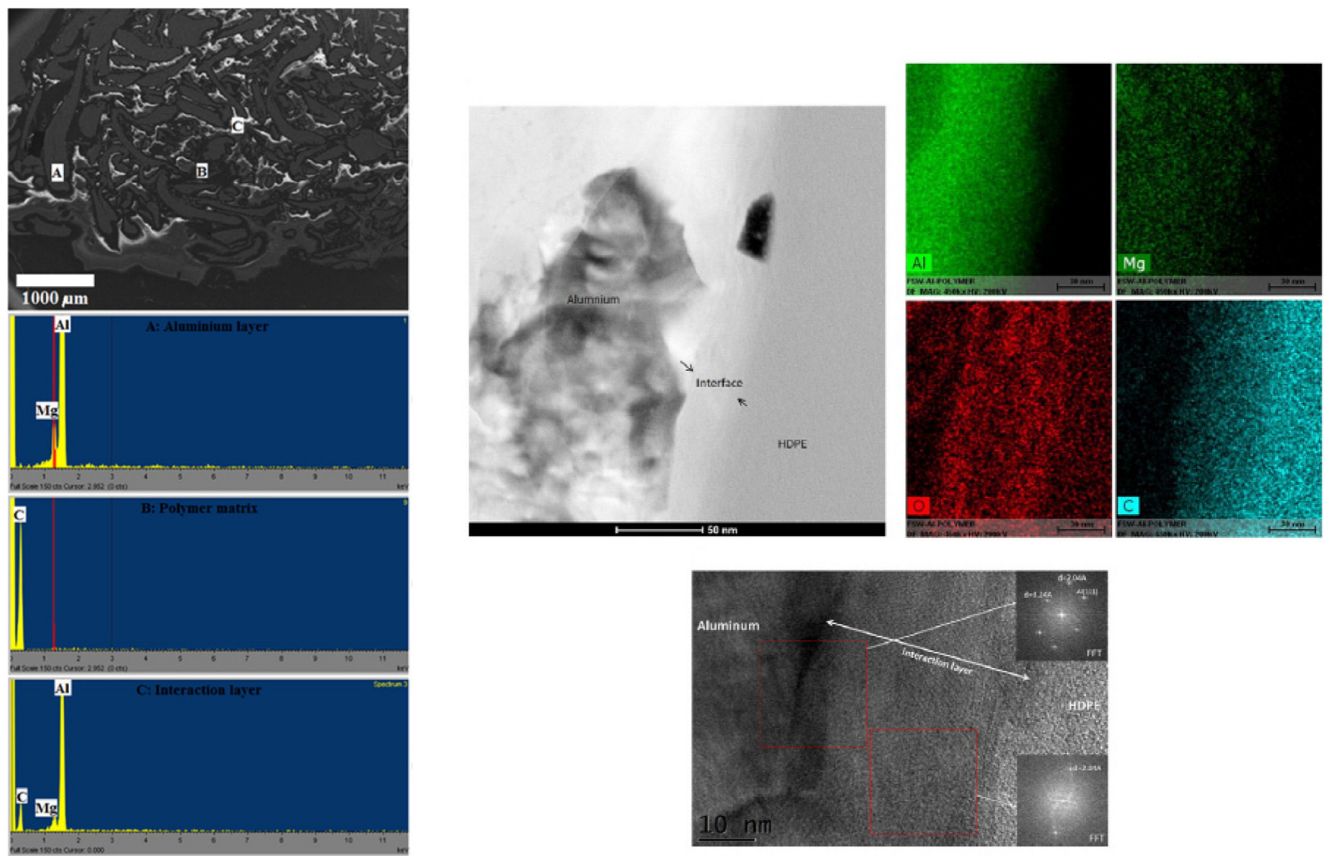


Fig. 9 TEM images of aluminum–polymer interface including the element mapping analysis and high-resolution TEM of the interface [42]

AA7075-polycarbonate Rahmat et al. [49] assessed the possibility of a hybrid FSW between aluminum 7075 and polycarbonate sheet using a 15° tapered probe of 3-mm length, 2-mm

diameter. Figure 6 shows the surface appearances of the welded joint. The welding parameter includes tool traverse and tool spinning rates of 200 mm/min and 4000 rev/min,

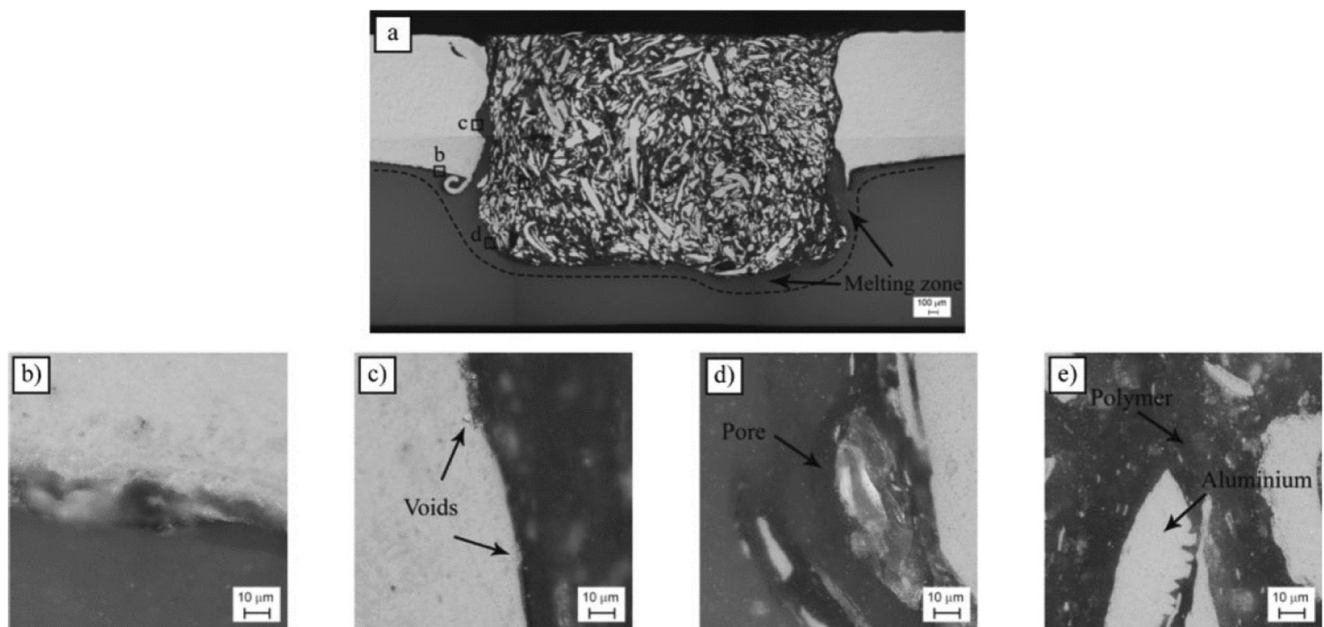
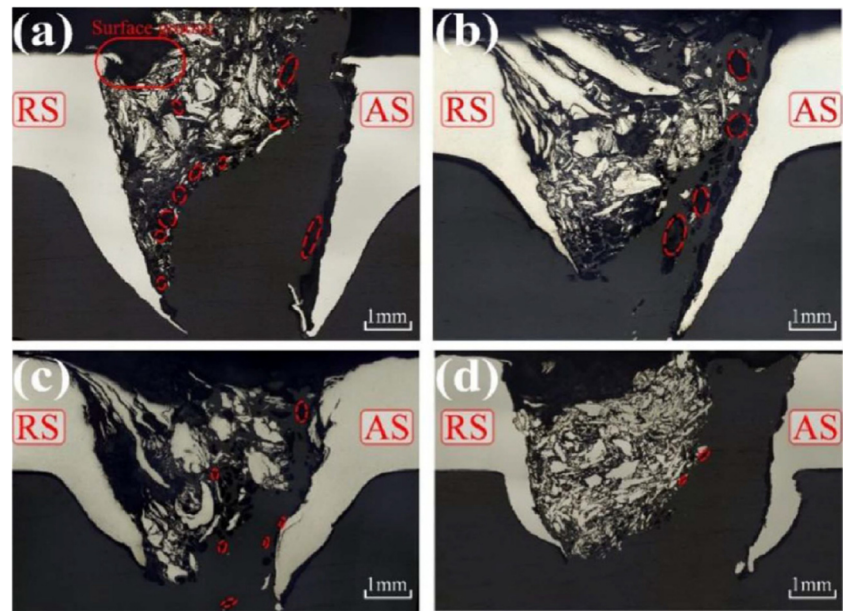


Fig. 10 (a) Optical microscopy images of the 6111–PPS stir zone (510 mm/min, 1200 rpm), (b) below aluminum sheet, (c) boundary area of aluminum SZ, (d) porosities inside the SZ, and (e) aluminum surrounded by PPS [41]

Fig. 11 Dissimilar weldments between aluminum and polymer at different traverse velocities of (a) 30 mm/min, (b) 50 mm/min, (c) 70 mm/min, and (d) 90 mm/min [45]



respectively. A valley-like structure with rough surface is formed in the surface of the weld, and this is due to downward force of the probe on the AA7075.

AA6111-polyphenylene sulfide Ratanathavorn and Melander [41] assessed the lap FSW between AA6111 and polyphenylene sulfide at a fix tool rotational speed of 1200 rpm and translational speeds of 10, 15, 20, and 25 mm/min. They used an H-13 tool steel as the FSW tool (threaded) with a 15-mm wiper shoulder. Figure 7 shows exterior look of the AA 6111–PPS joints. On the aluminum side, a rubbed surface with no flash is observed which is because of rotation and translation of the tool. The joined specimen contains a narrow path which is the fingerprint of the traveling FSW tool. Some slight sagging is observed on the back edge of the joint.

2.1.2 Materials inter-mixing, macro-flow pattern, and microstructure in the stir zone

To better understand the controlling mechanisms of the joint between polymer and metal in the FSW process, it is required to assess the stir zone more in detail and in higher magnifications. Figure 8 shows the stereographic images of the 5059 aluminum alloy and the HDPE mingling in the stir zone, studied by Khodabakhshi et al. [42]. It is visible from these images that metallic (Al) chips (fragments) are distributed in the soft polymer producing some hooks (locks). This is attributed to the non-uniform thermal gradient and non-homogeneous flow of the material in the advancing and retreating sides. Based on the Khodabakhshi et al. [42] findings, mechanical interlocking and chemical adhesion between the aluminum and resolidified polymeric layers are assumed as the main bonding

mechanisms in the butt welding of the AA5059 aluminum alloy and the HDPE. This is supplemented by indirect partial bonding ascribing to the Van der Waals interaction.

The aspects of metal/non-metal stir zone are provided in the SEM images in Fig. 9. Mechanical locking between aluminum and polymer matrix can be seen. Included in Fig. 9 is the EDS results from different zones which signify the elemental proof in these areas. It is evident that nearly a 30-nm thick layer is present at aluminum and HDPE interface. Elemental mapping analyses by Khodabakhshi et al. [42] showed that the interface contains a crystalline structure of aluminum with enhanced quantities of oxygen, and remnants of carbon (a nano-scale layer of corundum which is a crystalline form of Al_2O_3).

A similar observation was reported by Ratanathavorn and Melander [41] in overlap FSW of AA6111 and polyphenylene sulfide (PPS). Instead of plastic flow of the aluminum during the FSW of aluminum and polymer, due to lower process temperature, the aluminum material is cut through the FSW rotating tool and distributed within molten thermoplastic (i.e., PPS) matrix. These fragments along with relocated thermoplastic constitute the SZ; see Fig. 10.

Huang et al. [45] showed that the 6061-T6 aluminum anchor penetrates into the polyether ether ketone (PEEK) at the thermo-mechanically affected zone (TMAZ) of advancing side (AS) or retreating side (RS). They clearly explained the creation of Al anchors in the polymer matrix. The Al materials bend downward and penetrate the lap intersection as the polymer is readily deformed (softened), and further result in the generation of the Al anchors. The formation of Al hooks (anchors) is helpful to improve the strength (mechanical performance) of the joint. Huang et al. showed that the size and distribution of the aluminum anchors are related to the thermal

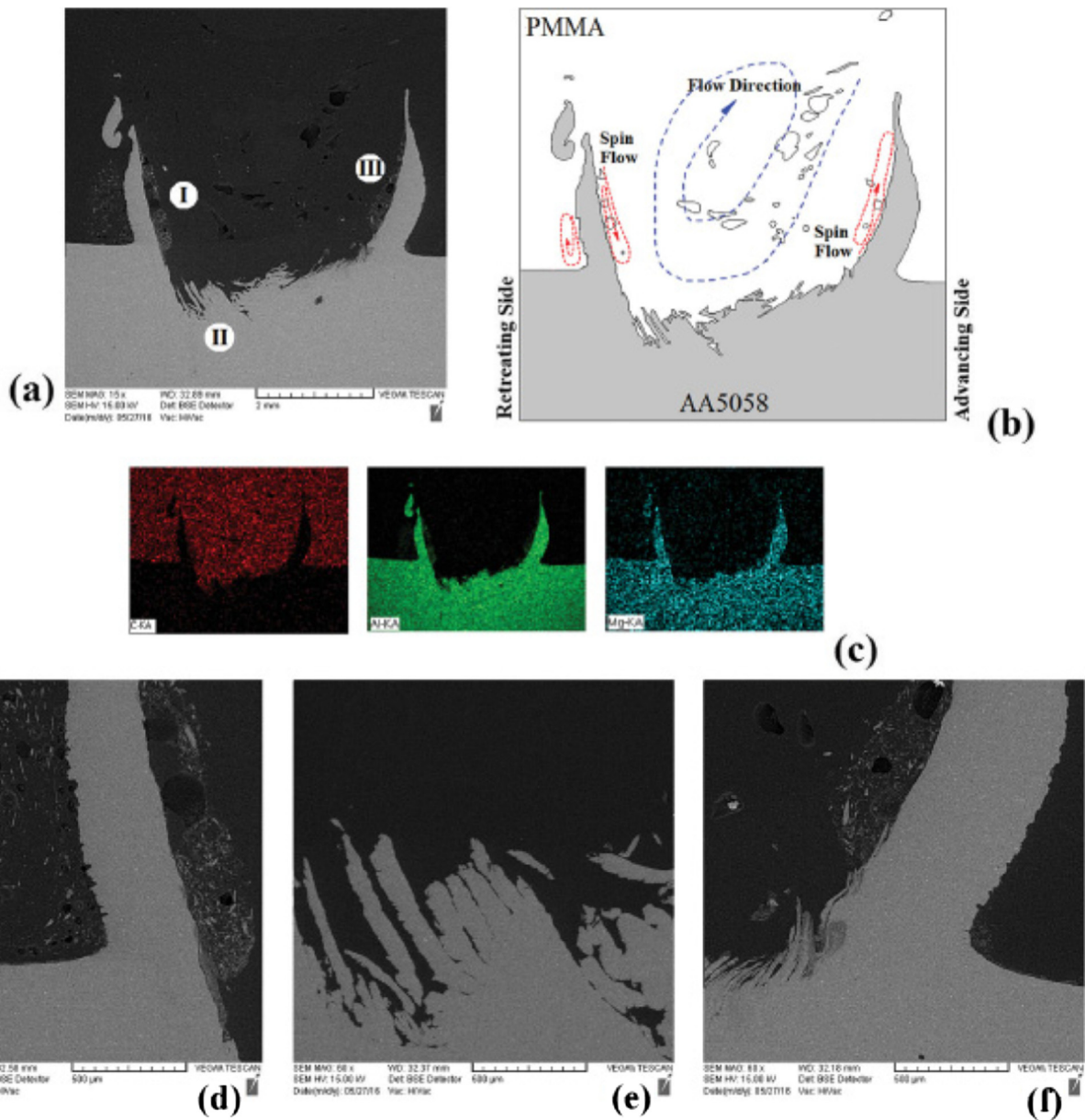


Fig. 12 Cross-sectional perspective of the divergent joint between AA5058 aluminum alloy and PMMA polymer opposite to FSW course. (a) SEM picture. (b) Schematic portrayal of materials stream example. (c)

Basic mapping compound investigation. SEM pictures from (d) withdrawing, (e) underneath, (f) and propelling sides of U tusk shaped in thickness segment amid different joint development [51]

gradient experienced during the welding operation. For instance, the size of the Al anchors is smaller in the retreating side than the advancing size. This is because of the higher temperature generated in the advanced side as compared with the retreating size. Figure 11 shows the zoomed in the structure of the metal/non-metal welds at various welding rates. The shearing and stirring action of the FSW tool result in breaking and mixing of aluminum and polymer pieces in the stir zone.

In separate studies, Derazkola et al. [50, 51] conducted a coupled mechanical modeling and experimental viability assessments on the FSW of an Al-Mg (AA5058) and poly-

methyl-methacrylate hybrid structures. They employed tool rotational speed of 1250 and 1600 rpm, tool traverse speed of 25 and 50 mm/min, with plunge depth and tool tilt angle of 0.2 mm and 2°, respectively. Through SEM images, they reported the formation of a U-shape antler which contains micro-lock (chips) from AA5058 toward the PMMA (see Fig. 12). They performed elemental mapping of the stir zone which showed the presence of Al, Mg, and tiny particles of carbon-rich phases in the U-shape anchor (see Fig. 12). However, the size, distribution, and morphology of aluminum chips in the stir zone are quite non-uniform, and this is because of variation in the temperature distribution in the advancing

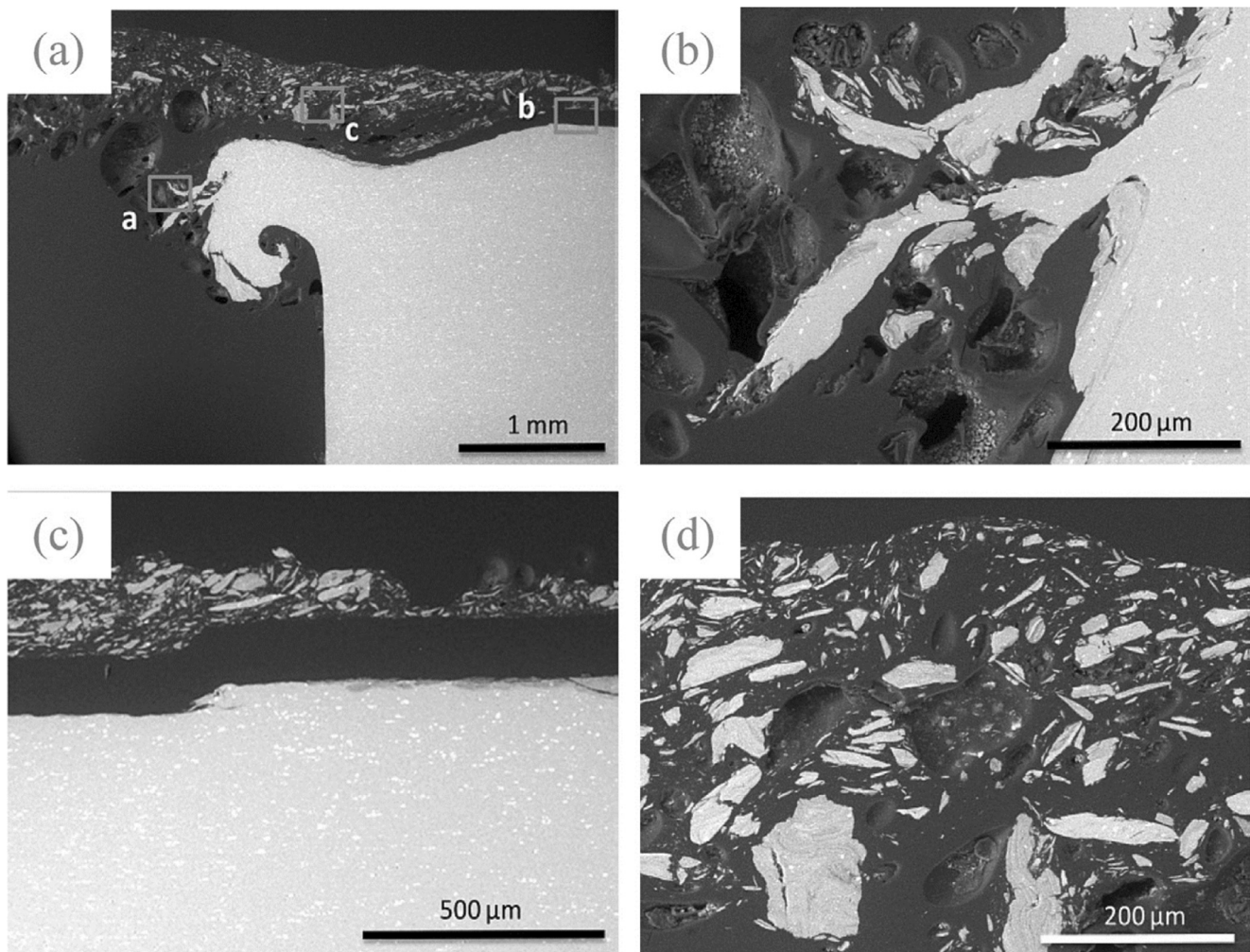


Fig. 13 SEM pictures demonstrating the cross-sectional between blending among aluminum and polymer amid FSW joining [46]

and retreating sides. The wavy micro-mechanical locking in the interface the aluminum and the polymer along with a layered lamella structure of aluminum and polymer directly contribute to the strength and performance of the joint.

Moshwan et al. [47] performed an introductory assessment on the FSW between aluminum 7075 and PC sheet (thickness of 3 mm) employing a welding tool with diameters of shoulder and pin; pin length was 9 mm, 1 mm, and 1 mm, respectively. They reported sound joints between 7075 alloy and PC sheet induced through the frictional heat generated by the spinning tool. The 7075 alloy was fragmented by the cutting action of the rotation FSW tool and interlocked into the PC sheet. No evidence of carbide, hydride, or oxide compounds was observed in the stir zone, though, as well as no diffusion occurred at the joint interface. They reported mechanical interlocking of 7075 alloy and PC was the primary joining mechanism.

The PC–AA 7075 joint at a tool rotational speed of 3250 rpm and a traverse speed of 100 mm/min is shown in Fig. 13. As seen, the aluminum chips are translated and

interlocked into the polymer matrix which is induced by severe plastic deformation produced on the AA 7075 due to the cutting action of the stirring tool. The qualitative EDX mapping analysis of the micro-joint interface between the PC and AA7075 with the concentration profiles of Al, C, Mg, O, and Cu is shown in Fig. 14. A sharp variation of different elements at PC and AA 7075 alloy was observed, as shown in Fig. 14. Al particles were scattered around the stir zone and spread toward the PC adjacent to the kissing bond of AA 7075 transportation.

2.1.3 Mechanical properties

Tensile strength A few scientists have directed uniaxial ductile testing to survey the execution of metal/polymer joints accomplished in the FSW procedure. For example, Derazkola et al. [50] demonstrated that with expanding instrument tilting point in the scope of 0° – 2° at a steady dive profundity, a definitive elasticity increments persistently (Fig. 15). Be that as it may, with expanding apparatus dive

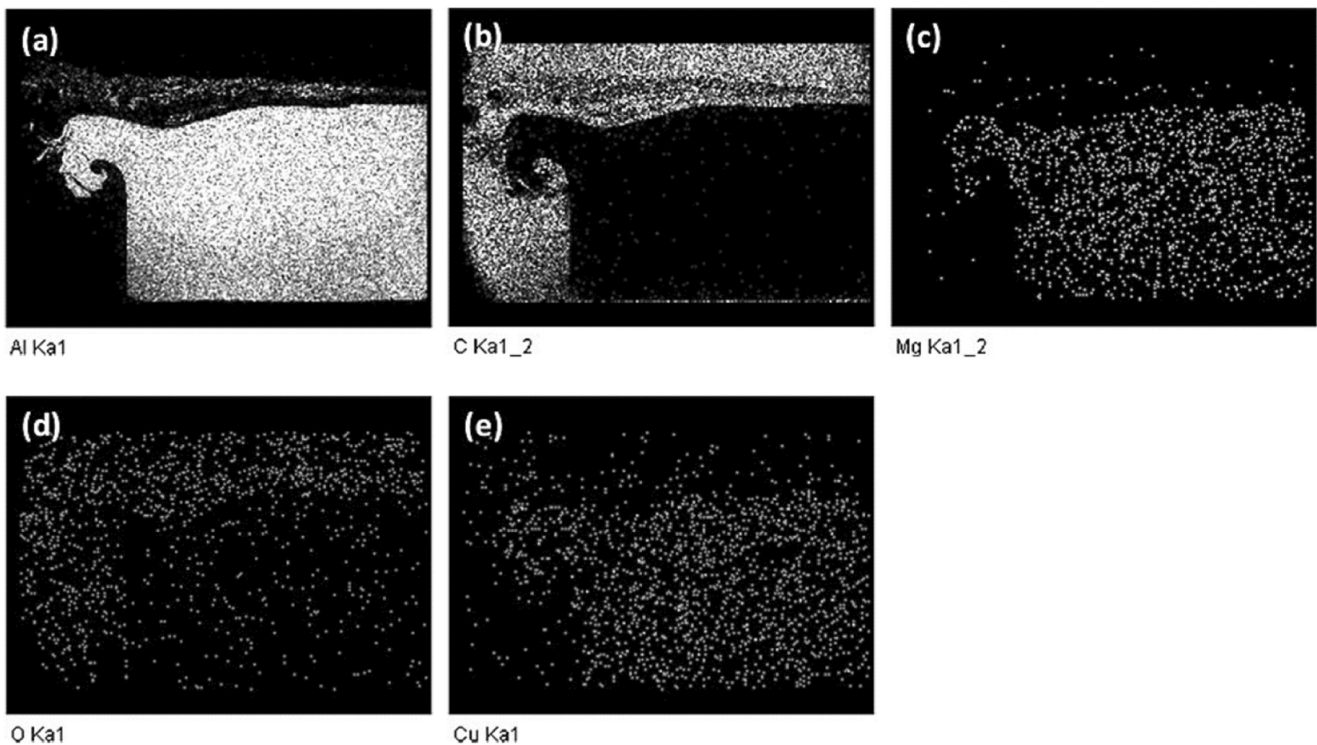


Fig. 14 Qualitative EDS mapping analysis of micro joint interface between PC and AA7075. (a) Al. (b) C. (c) Mg. (d) O. (e) Cu [47]

profundity in the scope of 0.1–0.4 mm, elasticity is expanded at first up to 0.2 mm and from there on decreased. As clarified previously, apparatus tilting edge and dive profundity as two principle preparing parameters are controlled by material stream and development of unique weld chunk.

Likewise, high dive profundity of 0.4 mm has a deteriorative effect on the joint quality because of exorbitant warming, the wrong arrangement of large-scale and smaller-scale

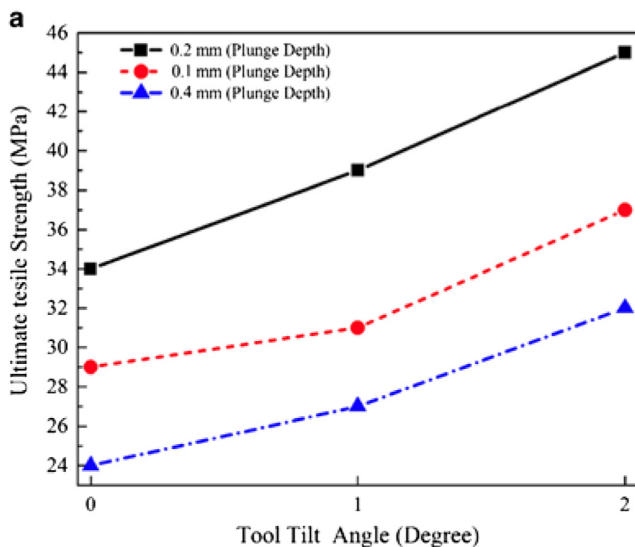


Fig. 15 Effects of tool tilt angle and plunge depth on the ultimate tensile strength of the processed dissimilar joints between AA5058 aluminum alloy and PMMA polymer [50]

mechanical interlocks, development of interior and surface deformities, and high volume portion of enormous air bubbles. As can be discovered, the most extreme rigidity is around 45 MPa which achieved at a device tilting edge of 2° and a dive profundity of 0.2 mm.

In a different report, Derazkola et al. [51] evaluated the ductile properties of the FSW joint between AA5058 aluminum-magnesium composite and polymethyl-methacrylate (PMMA). They saw that with expanding the apparatus rotational speed as well as diminishing the transverse speed, the quality of the joint builds (Fig. 16). This uncovers with increment in the warmth input, and materials between blending and between securing are advanced coming about improved mechanical properties. In their examination, a greatest joint quality of 45.5 MPa was gotten at $w = 1250$ rev/min and $v = 50$ mm/min.

Figure 17 incorporates the shear band quality (SBS) of an aluminum 6061-T6 amalgam and polyether ether ketone (PEEK) by means of contact blend lap welding (FSLW) contemplated by Huang et al. [45]. The SBS is tenderly affected by the microstructure (and warmth contribution) of the joint. Huang et al. [45] demonstrated that there is an immediate connection between the SBS and the span of the aluminum stays in the re-hardened polymer framework. As indicated by their investigation, with increment in the welding speed (up to 50 mm/min), the SBS increments. In any case, with further increment in the welding speed, as the measure of the aluminum stays diminishes, a drop in the SBS is seen, as the

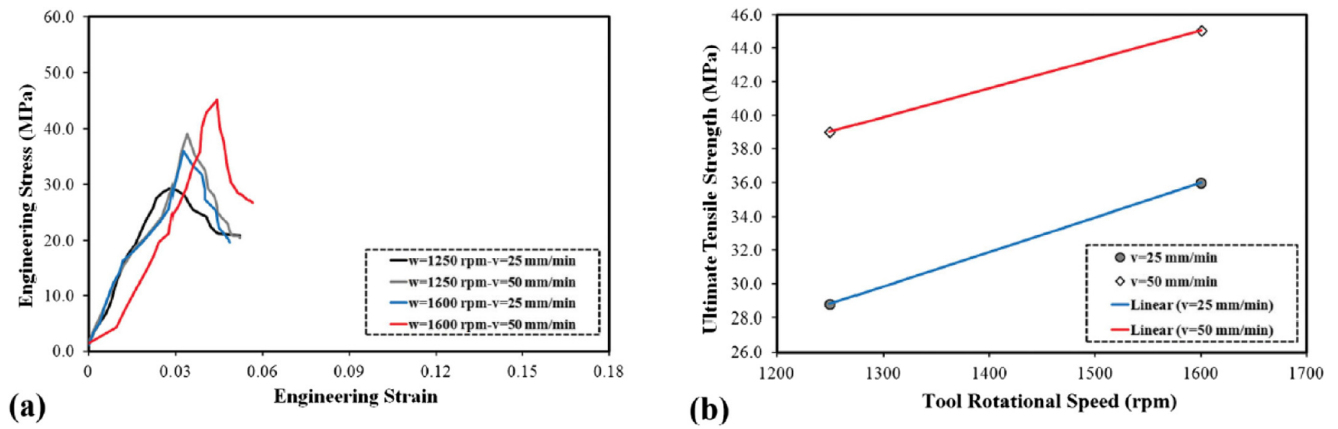


Fig. 16 (a) Engineering stress-strain plots for transverse elastic tried unique joints between AA5058 and PMMA. (b) Effects of the rotational speed at various navigate speed on the joint quality of different joints [51]

mechanical interlocking instigated by the moderately littler Al grapple is increasingly helpless. Table 2 condenses the shear bond qualities of different polymer/metal mixture lap joints gotten by various procedures.

Liu et al. [13] evaluated coordinate joining between AZ31B Mg compound and MC Nylon 6 utilizing erosion lap welding over an extensive variety of welding parameters. Table 3 gives the FSW parameters and the example assignment utilized by Liu et al. [13].

Figure 18 demonstrates the malleable shear test consequences of their FSW joints. As observed, with an expansion in the rotational speed, a decline in the welding speed, and an expansion dive profundity, the tractable shear quality disappointment stack (TSSFL) increments. This is straightforwardly identified with the warmth input created amid welding which shifts with diminishing or expanding the referenced parameter.

Khodabakhshi et al. [42] in their studies observed significantly different flow response and tensile strength in the

AA5059 ally (355 MPa) and the HDPE (20 MPa); see Fig. 19. They reported that the dissimilar AA5059/HDPE joint possesses a joint efficiency of 50% relative to the HDPE base material which indicates some promising bonding strength at the interface. Various factors may contribute to the reduced strength of the joint relative to the HDPE; these include stress concentration in the edges of aluminum chips in the re-solidified HDPE, formation of shrinkage micro-voids, and weaker interfacial bonding.

Liu et al. [13] showed that the FSW parameters possess a great influence on the nominal shear strength (NSS) of the FSW joints between MC Nylon-6 and AA6061. Figure 20 provides the nominal shear strength (NSS) of the FSW joints under different welding parameters. Looking at this graph one can conclude that (i) the NSS varies between 5 and 8 MPa under the studied parameters (tool travel speed and tool rotational speed) with the optimum strength at 200 mm/min, and (ii) at spinning speeds of 2000 and 3000 rpm, the NSS decreases continually with increasing the welding speed. The general trend in Fig. 20 shows that increasing the rpm can have a positive effect on the joint strength of the MC Nylon-6 and AA6061, while it is quite challenging to get reliable joints with acceptable strength at high welding speeds.

Moshwan et al. [47], who studied dissimilar friction stir welding between polycarbonate and AA 7075 aluminum alloy, assessed the effect of the FSW main parameters on the

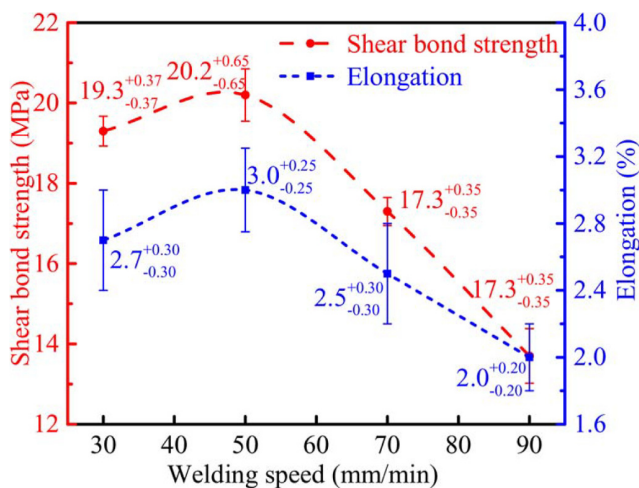


Fig. 17 Shear bond quality and lengthening of the aluminum-polymer joints by various welding speeds [45]

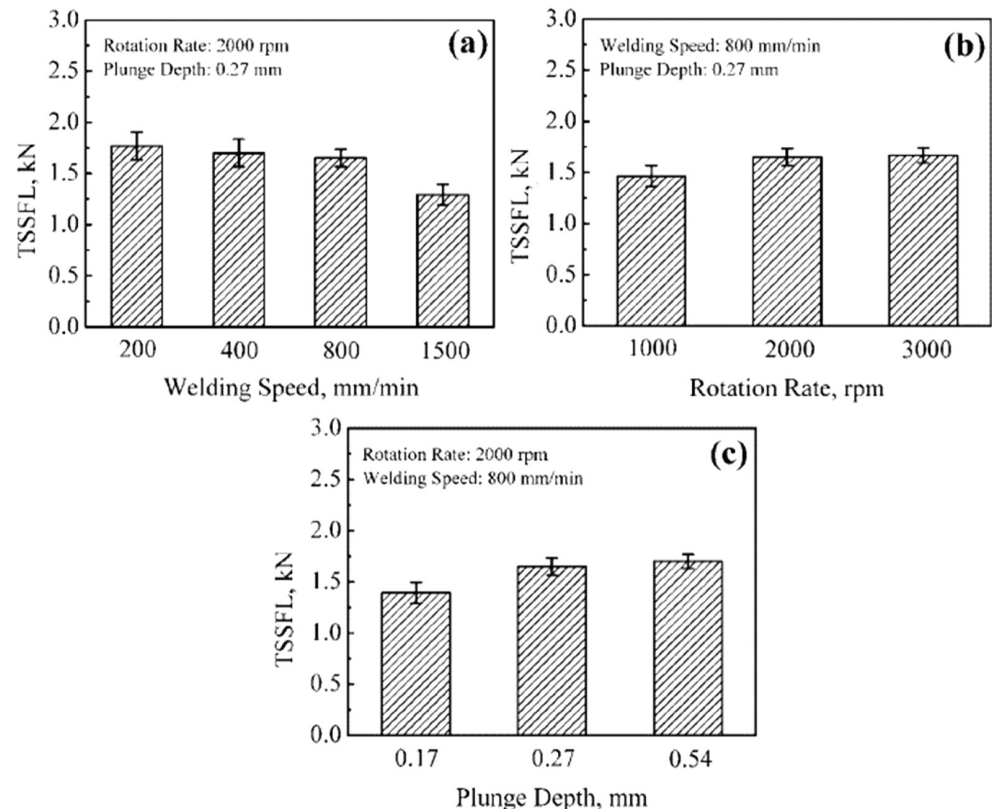
Table 2 Maximum SBS of various polymer-metal hybrid lap joints obtained by different conditions of FSW technique [45]

Maximum strength	Dissimilar joint ratio	Tool design
12.9 MPa	9.2%	A pinless tool
5.75 MPa	9.3%	A cylindrical threaded pin
5.1 MPa	16.3%	A threaded tapered pin
20 MPa	20.6%	A tapered thread pin with the triple facets

Table 3 Welding parameters and test assignments for FLW joints of AZ31B/MC Nylon 6 [13]

Shoulder diameter (mm)	Plunge depth (mm)	w (rpm)	v (mm/min)
15	0.27	2000	200
15	0.27	2000	400
15	0.27	2000	800
15	0.27	2000	1500
15	0.27	1000	800
15	0.27	3000	800
15	0.17	2000	800
15	0.54	2000	800
15	0.27	4000	1500
15	0.54	4000	1500
15	0.81	4000	1500

tensile strength and elongation of the friction stir welded joints. They ran nine FSW experiments with rotational speeds of 300, 3250, and 3500 rpm and traverse speed of 50, 100, and 150 mm/min. They found that the strength of the welded joint was less than 10% of the PC base material which is tangibly less than what reported by Khodabakhshi et al. [42]. They reported the optimum strength and ductility properties in the samples welded under 3250 rpm and 100 mm/min condition; see Fig. 21.

Fig. 18 Tensile shear properties of FLW joints delivered at various (a) welding speed, (b) instrument turn rate, and (c) device dive profundity [13]

Rahmat et al. [49] reported tensile properties of FSW lap joints between 7075 aluminum alloy and polycarbonate sheets. They kept the spindle speed constant at 3250 rpm while changing traverse speed (50 to 150 mm/min) and depth of tool shoulder penetration (0.10 to 0.30 mm). Table 4 provides a summary of maximum tensile load, ultimate tensile strength, and elongation of various welds (FSW_a, FSW_b, FSW_c, and FSW_d). They reported an optimum condition when employing traverse speed of 100 mm/min and depth of penetration of 0.2 mm. This gives a peak tensile load of 183.38 N (equal to ultimate tensile strength of 4.72 MPa). This is less than 10% of the PC base metal strength.

Microhardness Indentation microhardness measurement is a great tool to assess the local properties of the metal-polymer FSW joints in the base materials (BM), heat-affected zone (HAZ), thermomechanically affected zone (TMAZ), and the stir zone (SZ). This may not be necessarily feasible in the uniaxial tensile testing. Therefore, a number of researchers have assessed the joint performance through indentation hardness testing. To this end, Khodanakhshi et al. [42] ran instrumented indentation Vickers hardness testing on the AA5059/HDPE joint and showed that hardness increases by moving from the HDPE base material (4.6 VHN) toward the AA5059 aluminum base (86.7 VHN), as shown in Fig. 22. They reported the hardness of the SZ and the AA5059/HDPE

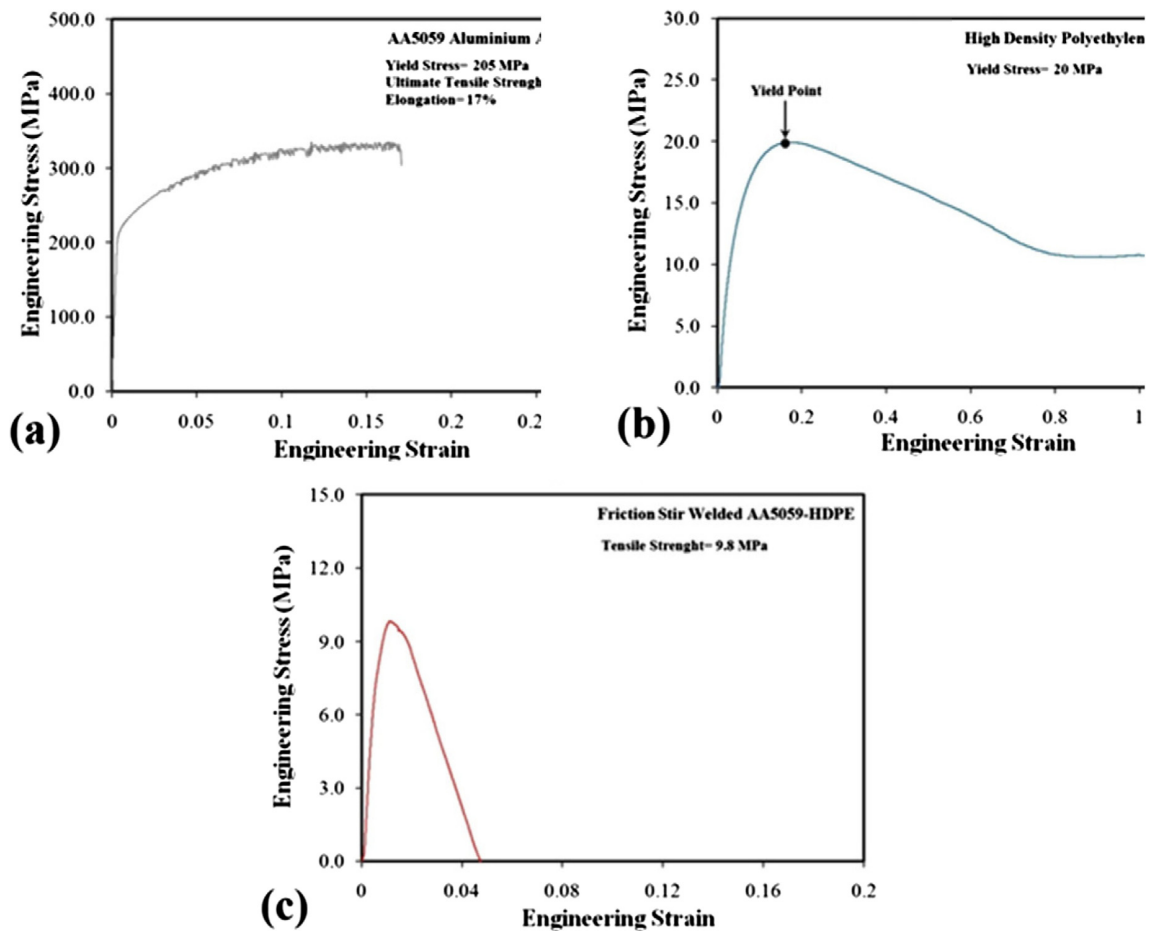


Fig. 19 Engineering stress–strain curves for (a) AA5059, (b) HDPE, and (c) friction stir welded Al–HDPE [42]

interface as 10.4 and 6.8 VHN, respectively. The enhanced hardness (by approximately 100%) of the SZ as compared with the HDPE base material is because of the presence of aluminum chips (fragments) in the SZ (aluminum fragments distributed in the re-solidified HDPE).

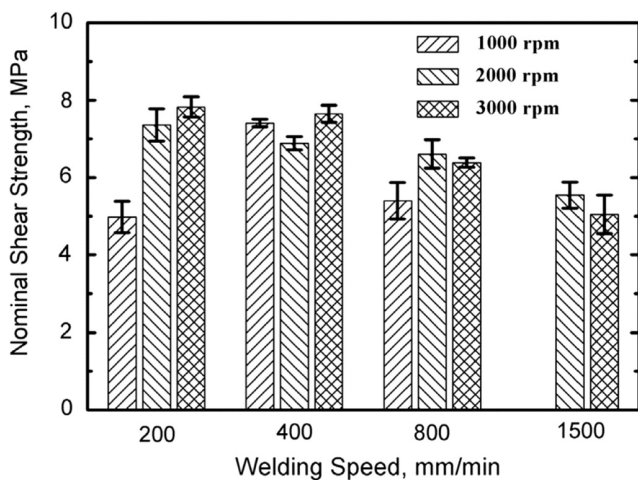
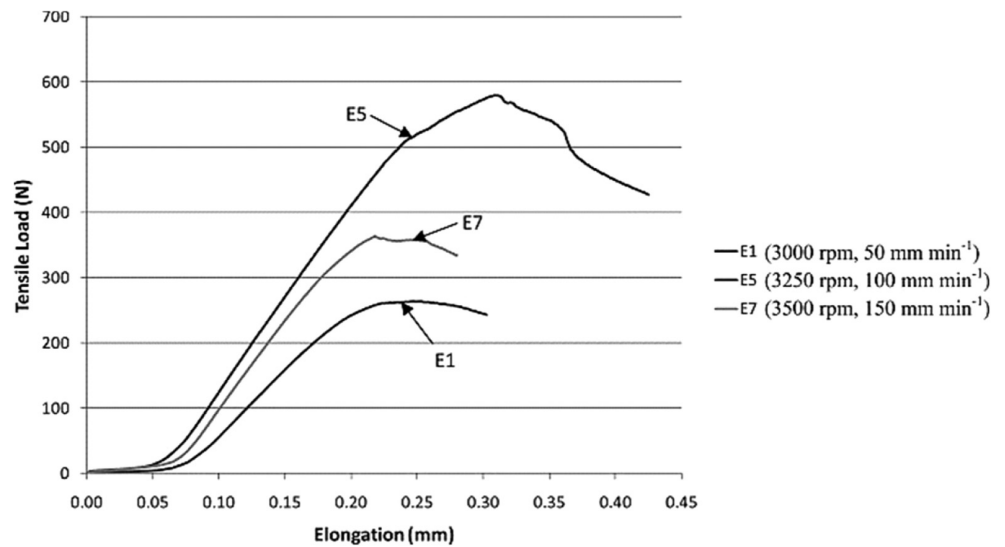


Fig. 20 Nominal shear test aftereffects of FLW joints of MC Nylon-6 to AA6061 welded under different parameters [13]

Figure 23 displays the microhardness dispersions at various welding areas in the erosion mix lap welding of 6061-T6 aluminum (Al) combination and polyether ether ketone (PEEK). An uneven conveyance in the hardness is seen with the pinnacle estimation of 98 VHN in the BM of the 6061-T6 amalgam and minimal estimation of 15.2 HVN in the liquid and re-set PEEK of the SZ. This was credited to the loss of the sub-atomic weight and the decrease of the crystallinity of the PEEK in the mixing zone which encounters an extreme twisting and warm angle. Since aluminum chips are installed in the liquid and re-hardened PEEK amid the FSW procedure, the normal hardness of the SZ is higher than the BM of PEEK, while lower than BM of 6061-T6 Al. This is in concurrence with what Khodabakhshi et al. [42] and Shahmiri et al. [52] have detailed.

Derazkola and Elyasi [44] considered the Shore D and the Vickers hardness dispersion in the lap-joint FSW of the AA5058 and the polycarbonate (PC) sheets. Figure 24 contains a schematic perspective of the hardness test lines in the PC and the AA5058 composite (Fig. 24a) and additionally hardness variety of the FSW PC and AA5058 composite at different device rotational rates (Fig. 24b, c). It is seen that the hardness values of the FSW processed PC

Fig. 21 Tensile load curve of dissimilar weldments between AA7075 and PC for highest, middle, and lowest load for E5, E7, and E1, respectively [47]



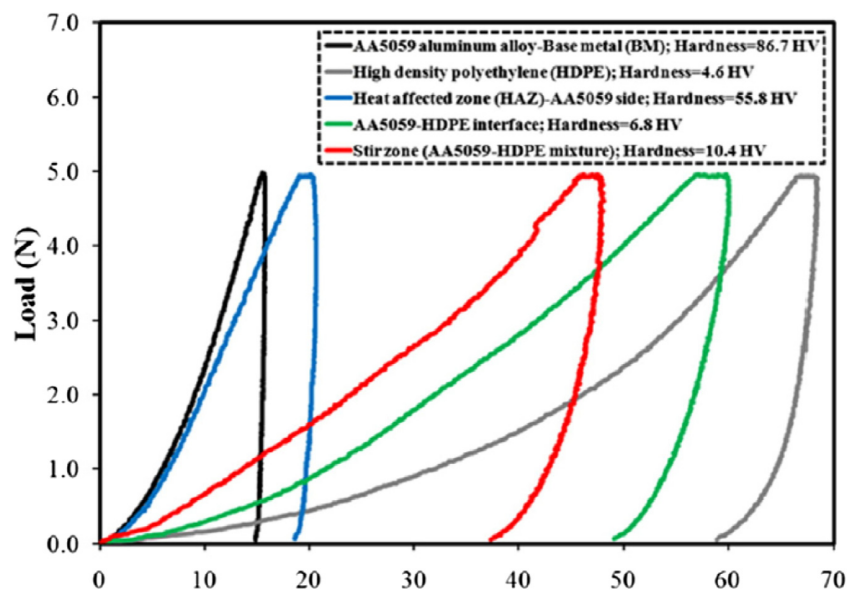
are less than the primary (unprocessed) PC sheet. This can be attributed to the change in the molecular structure and molecular weight due to the fictional heat input of the FSW process. However, the microhardness of the processed AA5058 is improved thanks to the grain refinement induced via the FSW process.

According to Moshwan et al. [47] studies on dissimilar friction stir welding between polycarbonate and AA 7075 aluminum alloy, the lowest hardness value of 6.6 HV_{0.025} was obtained at 1 mm on the PC side, while this is 120 HV_{0.5} at the 0.75 mm on the AA7075 side; see Fig. 25. They watched a reasonable hardness decrease in the welded

Table 4 Main tensile properties of the produced PC-AA7075 dissimilar joints by FSW process [49]

Shoulder penetration (<i>D</i> , mm)	<i>v</i> (mm/min)	<i>D/v</i> (%)	<i>F</i> _{max} (N)	Elongation (%)	UTS (MPa)
0.05	150	0.03	165.60	0.0704	2.76
0.10	100	0.10	243.06	0.1878	4.05
0.20	100	0.20	283.38	0.1800	4.72
0.30	50	0.6	260.66	0.1334	4.34

Fig. 22 Indentation hardness load–depth graphs for BMs AA5059, HDPE, HAZ, and SZ [42]



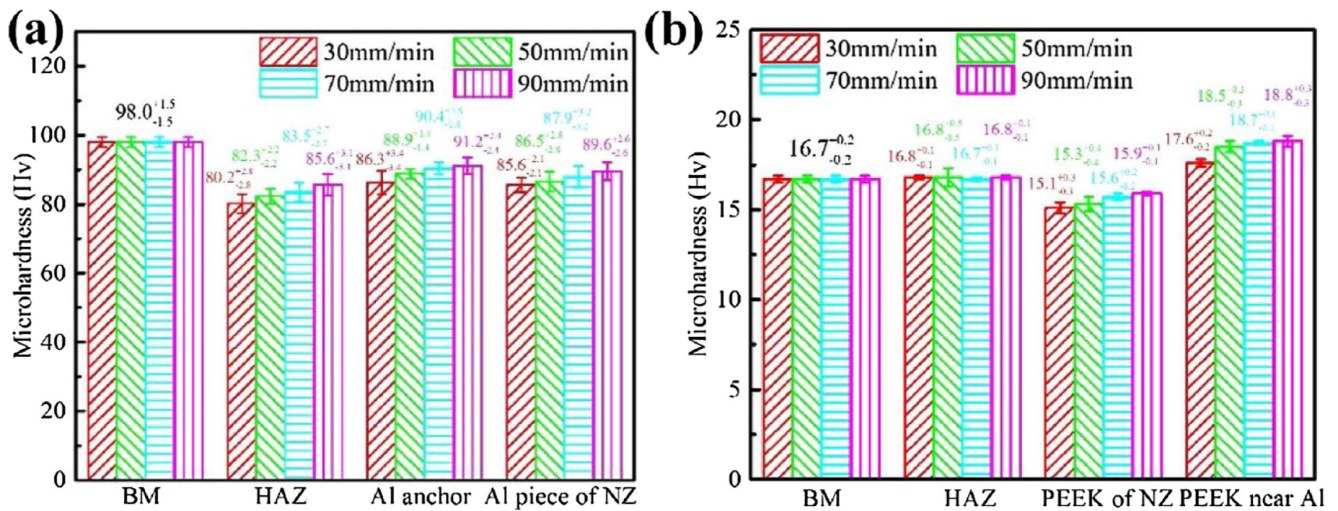


Fig. 23 Microhardness appropriations of the commonplace joints between AA6061 alloy and PP polymer. (a) 6061-T6 Al composite. (b) PEEK [52]

territory of the PC side which is actuated by warm debasement in the polymer. This is in concurrence with the recently detailed hardness esteems for disparate metal/polymer joints [47].

Same observations, hardness reduction in the welded area of the polymer side caused by thermal degradation due to the tool stirring and frictional heat, were reported by Patel et al.

[48] in assessing the microhardness of the FSW joints between the AA6061 and the PC (see Fig. 26).

Figure 27 gives the impact of the FSW parameters on the hardness esteems and the grain size of AZ31B Mg amalgam and MC Nylon 6 plates, performed by Liu et al. [13]. As seen with an expansion in the welding speed from 200 to 1500 mm/

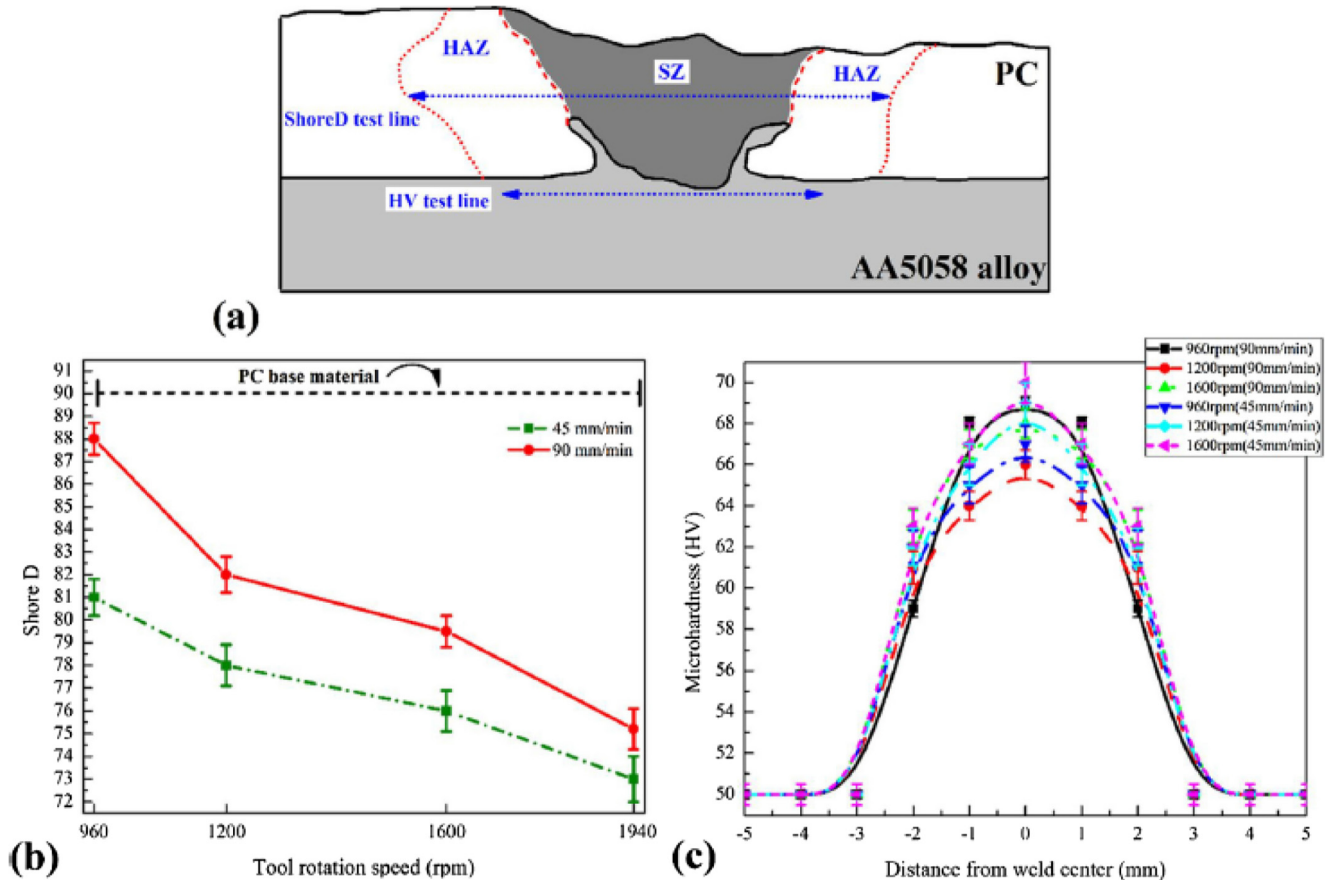


Fig. 24 (a) Schematic view from hardness test line at PC and AA5058 composite. (b) Aftereffects of hardness changes (shore D) in PC side. (c) Consequences of hardness changes (HV) in AA5058 combination side [44]

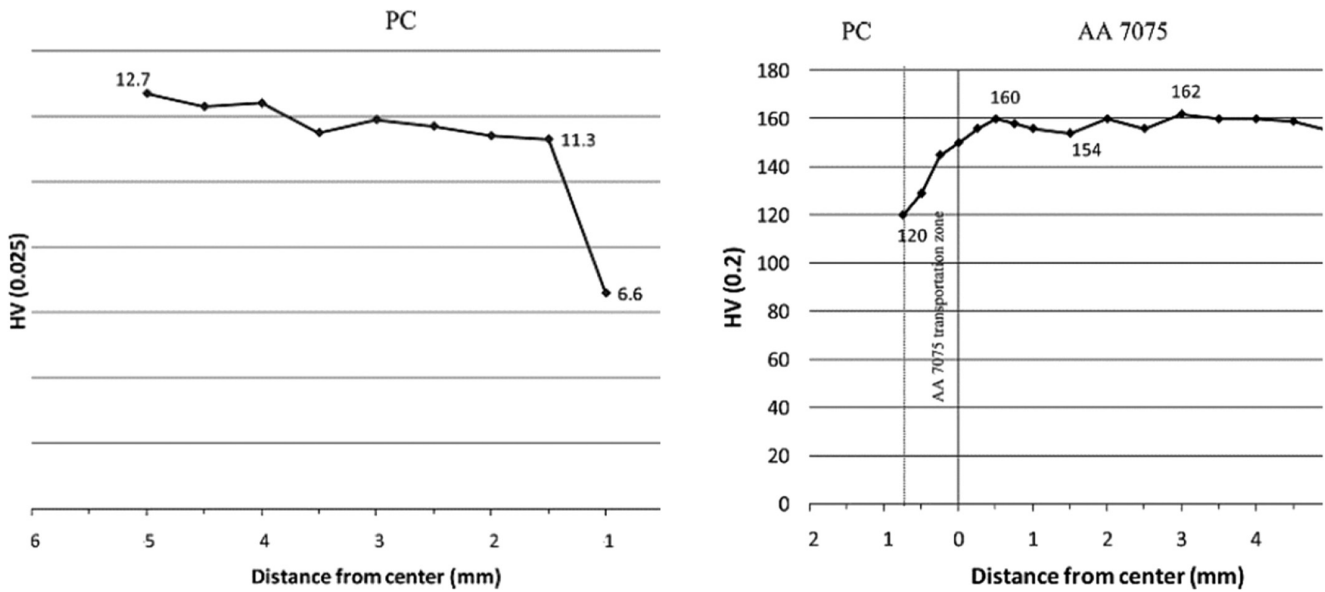


Fig. 25 Vickers microhardness at PC joint interface (left). Vickers microhardness at AA7075 base material and the interface (right) [47]

min, a decline in the instrument rotational speed from 3000 to 1000 rpm, and decline in the dive profundity from 0.54 to 0.71, the Vickers hardness increment. This is straightforwardly identified with the adjustment in warmth contribution with change in the welding parameters.

Fracture studies Figure 28 provides macro-images of the fractured tensile specimen in the Khodabakhshi et al. [42] research work on the FSW of AA5059/HDPE. As observed, the failure location is at the interface between the stir zone and the AA5059 base metal and not necessarily in the stir zone. They also performed SEM fractography on the fracture surface, and though EDS analyses (see Fig. 29) showed some bonding between the HDPE and the AA5059 (fracture surface contains aluminum and adhered polymer material). This clearly provides further evidence of bonding between aluminum and polymer through the FSW process.

Ratanathavorn and Melander [41] reported a two-step shear fracture in the overlap FSW between AA 6111 and PPS. According to the cross section of the fracture specimen and

the failure load curve, see Fig. 30, fracture first starts at the location I and propagates along the interface of the SZ and the aluminum sheet. The crack propagation leads to a reduction in the load at point A; see Fig. 30a. This is followed by a secondary crack (II) which is initiated between the SZ and the polymer (PPS). This results in a second load drop observed in the load failure curve.

In light of the nylon conveyance, Liu et al. [13] partitioned the morphology of the fracture surfaces of t MC Nylon-6 to AA6061 joint into seven zones (qualified Zone I for Zone VII). Figure 31 demonstrates the optical pictures of the fracture surfaces of the half and half joints created by FLW at 2000 rpm and different welding speeds. These zones incorporate Spherulite morphology (Zone I), disfigured nylon (Zone II), lingering nylon (Zone III), AA6061 surfaces (Zone IV), and the edge formed nylons (Zones V, VI, and VII). The morphology of edge molded nylons can be viewed as a marker of the fracture proliferation ways in the nylon amid malleable test (this appears in Fig. 32). Factual examination demonstrated that the shear quality bearing capacity of these locales ought to

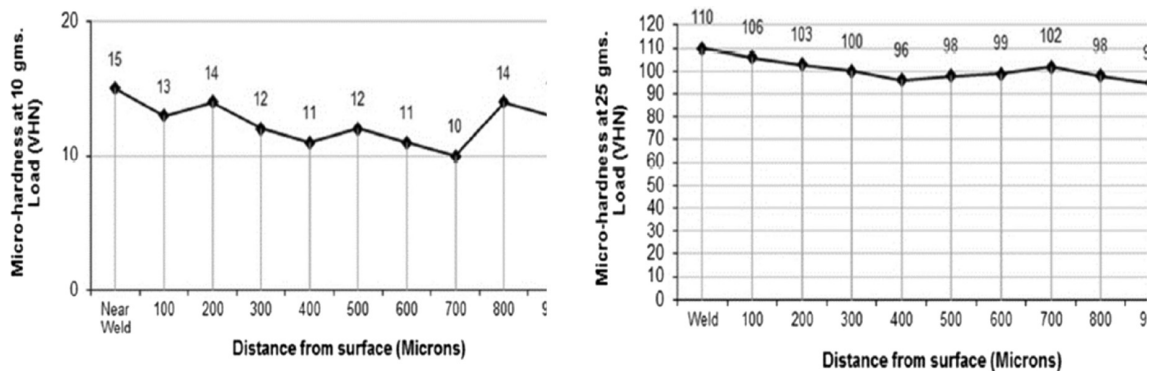


Fig. 26 Profile of micro-hardness plot (left) PC side (right) AA 6061 side [48]

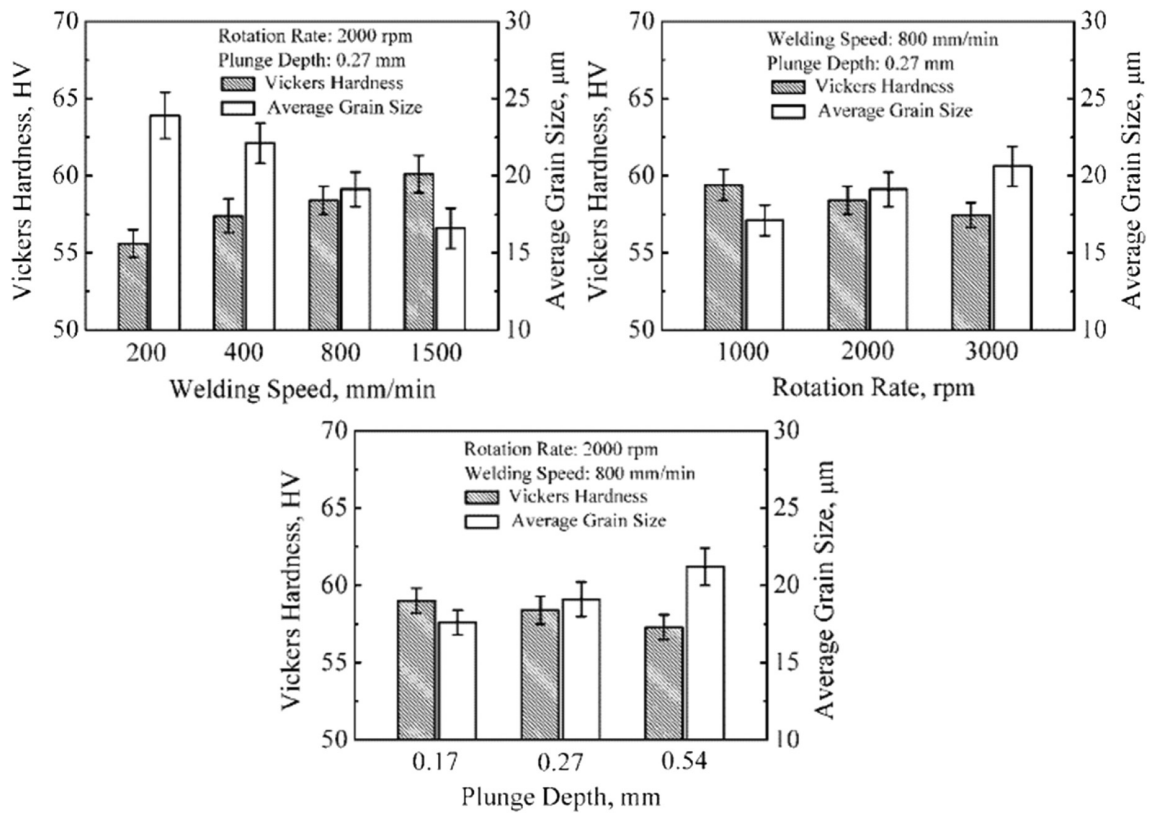


Fig. 27 Variation in Vickers hardness and average grain size with (a) welding speed, (b) rotation rate, and (c) plunge depth [13]

pursue such a request: district II > region V > area VI > area VII > locale IV > area I or III.

The fracture characteristics of FSWed AA5058-PMMA lap-joint, studied by Derazkola et al. [50], are shown in Fig. 33. It is observed that the fracture line is located at the interface of the stir zone and the U-antler near the PMMA, in the retreating side (zone II).

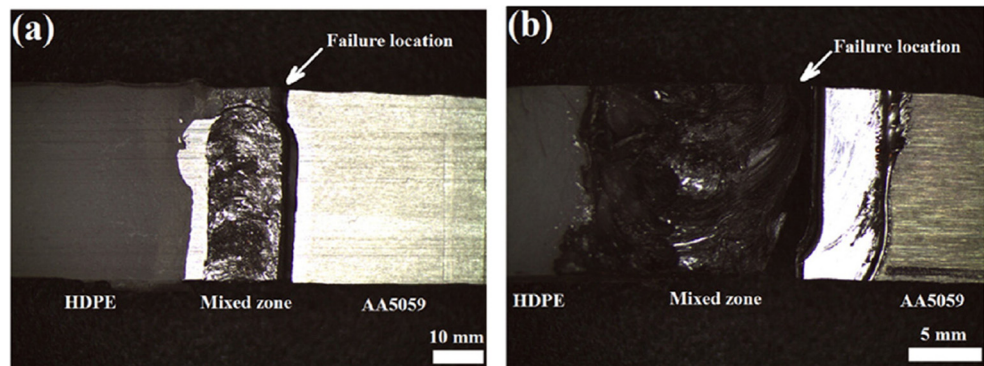
The crack area in the FSW of 6061-T6 aluminum (Al) composite and polyether ether ketone (PEEK) was accounted for by Huang et al. [45], at the welding paces of 30 mm/min and 90 mm/min, which appeared in Fig. 34. As observed, fracture lies at the interface among metal and the liquid polymer at the mechanical interlocking locale of the propelling

size. With increment in the elastic stacking, the primary crack(s) quickly develop through the halfway glue holding zone among polymer and metallic base. At the point when aluminum keeps (stays) haul out of the SZ, the last crack occurs.

2.2 Friction-stir processing of aluminums and polymers

As explained in previous sections, large dissimilarity between aluminum and polymer is very challenging to reach a proper state in accomplishment of dissimilar joining between these materials. An impact difference between the mechanical

Fig. 28 Optical macrographs from the top surface view of failed FSW joint between AA5059 and HDPE following transverse tensile testing [42]



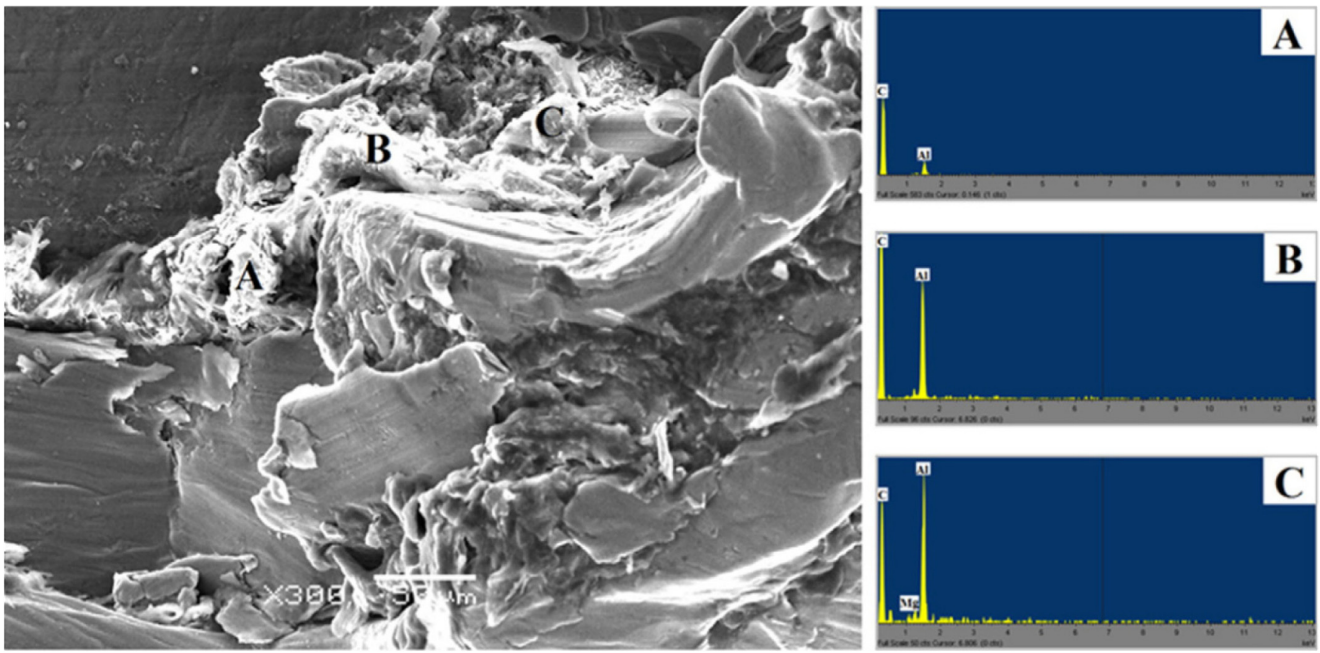


Fig. 29 FESEM image combined with related EDS spectra from the fracture surface of transversely tensile failed dissimilar Al–HDPE FSW joint [42]

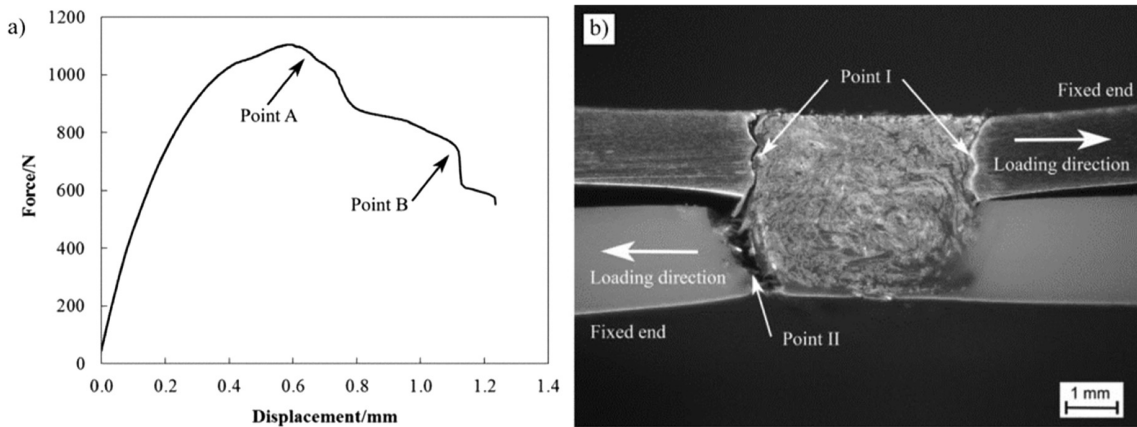


Fig. 30 (a) Typical failure load curve for AA6111-PPS dissimilar weldment. (b) Cross section of fracture specimen [41]

Fig. 31 Fractured surface observation for FLW joints of MC Nylon-6 to AA6061 welded at 2000 rpm and various welding speed: (a) 200 mm/min, (b) 400 mm/min, (c) 800 mm/min, and (d) 1500 mm/min [13]

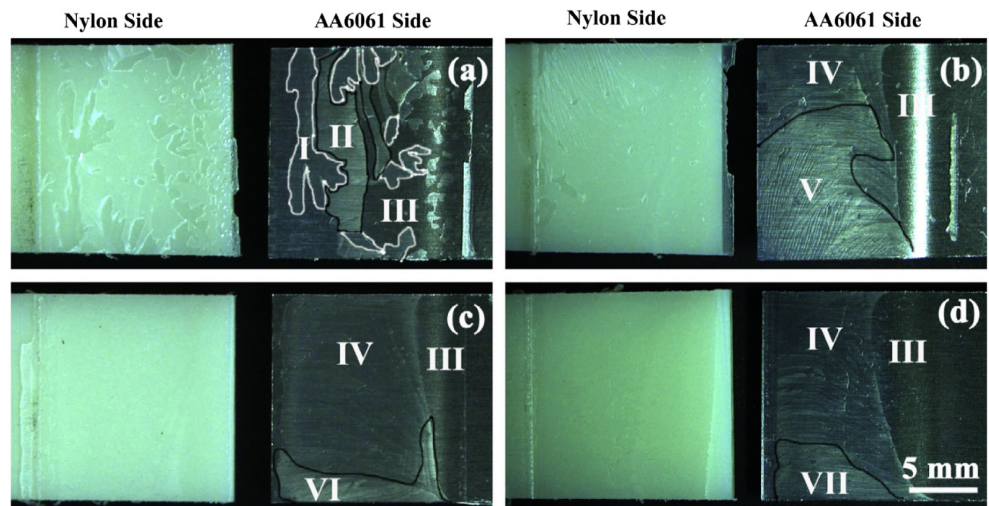


Fig. 32 Typical SEM images obtained from fracture surface of dissimilar AA6061-Nylon 6 weldment. (a) Low magnification. (b) High magnification [13]

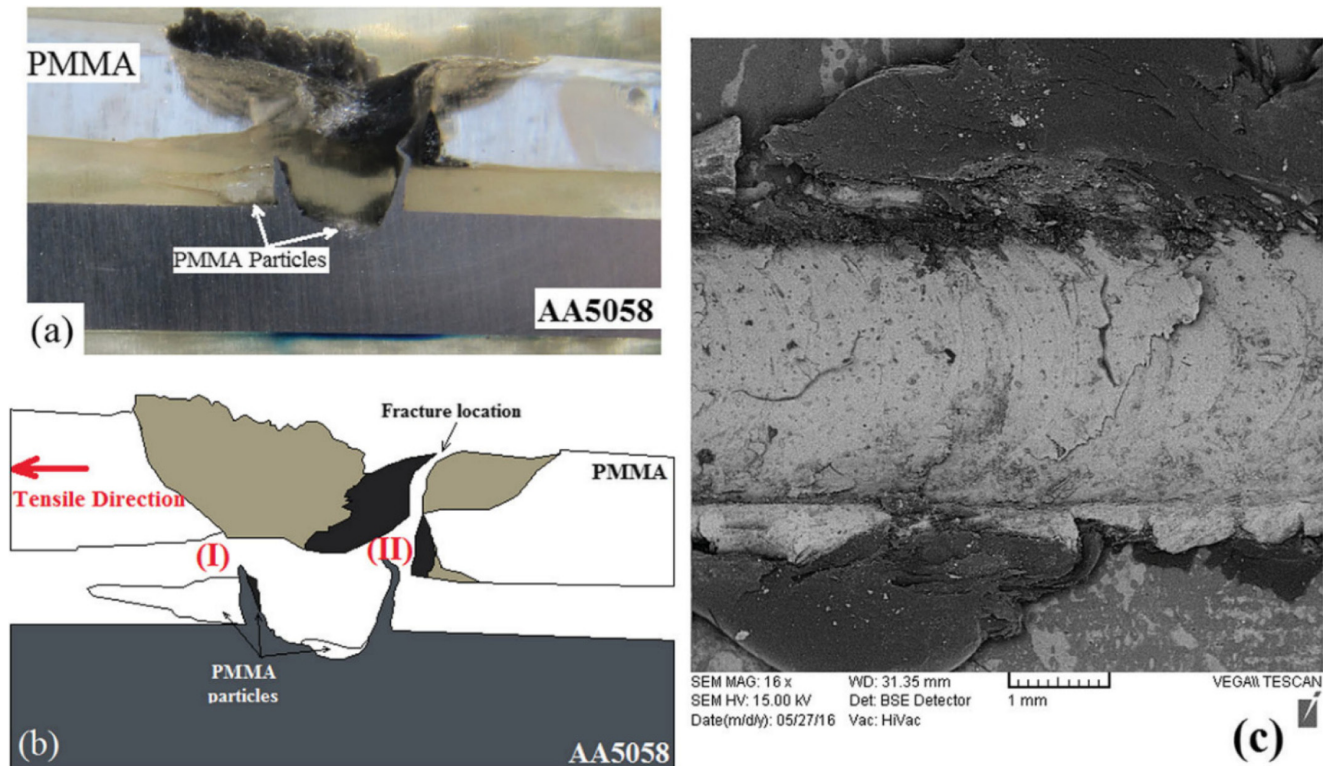
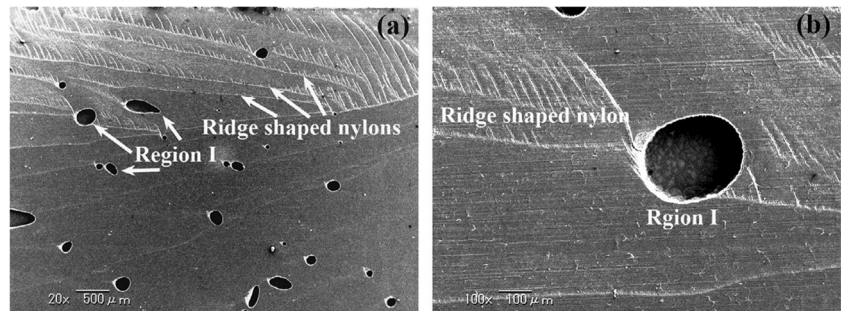


Fig. 33 Fracture behavior of the dissimilar FSWed AA5058-PMMA lap-joint. (a) A real failed sample. (b) Schematic representation of rupture accomplishment during tensile-shear loading. (c) Fractography features on the fracture surface [50]

strength is very determinative on deterioration of material flow and intermixing through the weld nugget. Depending on the type of aluminum alloy and polymer, in some cases, the hardness and tensile strength of aluminum can be more

than ten times higher than the polymer base material. As the same as physical property of aluminum in terms of electrical and thermal conductivity is extremely higher than polymer, they are very important to control the weld nugget formation

Fig. 34 Fracture locations of the hybrid joints between aluminum alloy and polymer at two different tool rotational speeds of (a) 30 mm/min and (b) 90 mm/min [45]

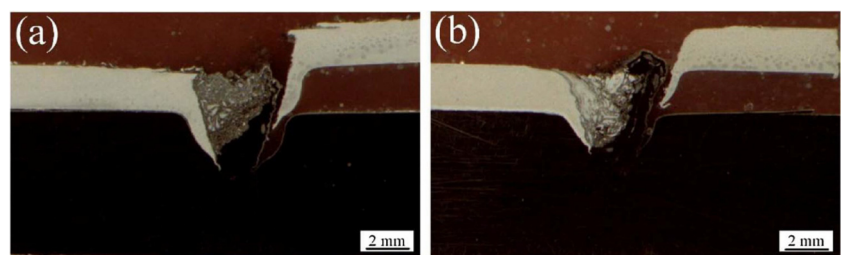
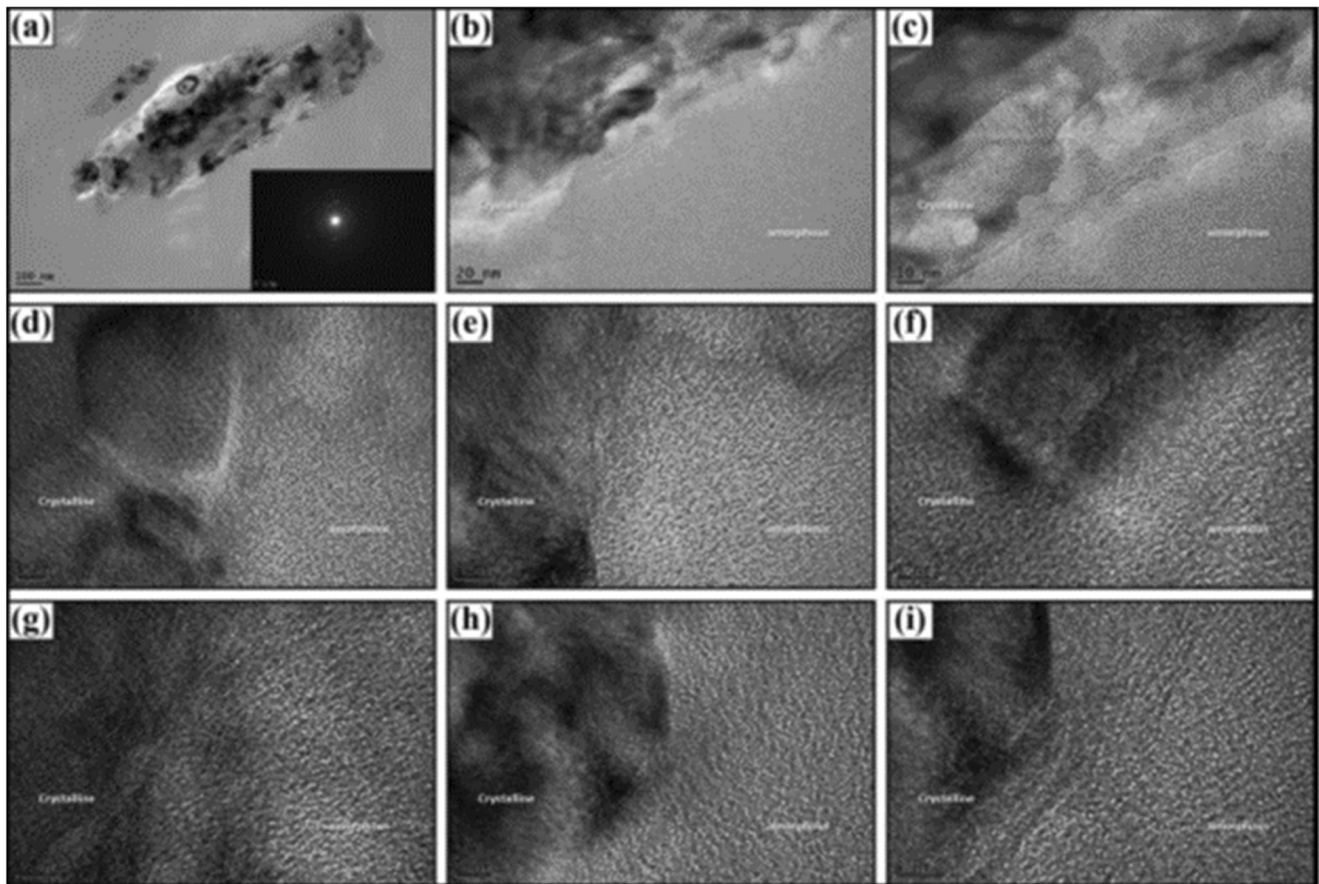


Table 5 Dissimilar joining efficiency for various processed dissimilar weldments by FSW

Dissimilar system	Joint design	Soundness	Strength ratio	Failure location	Reference
AA5059-HDPE	Butt	Shrinkage voids	~ 50%	SZ/aluminum interface	Khodabakhshi et al. [1]
AA5058-PMMA	Lap	Surface tunnels	~ 60%	SZ/aluminum interface	Derazkola et al. [50]
AA5058-PC	Lap	Bubbling	~ 68%	SZ/aluminum interface	Derazkola et al. [44]
AA6061-PC	Butt	Shrinkage voids	~ 34%	SZ/aluminum interface	Patel et al. [48]
AA6061-Nylon 6	Butt	Ridge shaped nylon	~ 30%	SZ/aluminum interface	Liu et al. [13]
AA7075-PC	Butt	Feeble intermixing	< 10%	SZ/aluminum interface	Rahmat et al. [49]
AA6111-PPS	Lap	Interfacial voids	~ 55%	SZ/aluminum interface	Ratanathavorn et al. [41]

during a thermo-mechanical based joining process such as FSW. Therefore, to compensate this large dissimilarity between aluminum and polymer, one effective way is reinforcing the polymer side with secondary phase agents to reduce the difference between physical and mechanical properties of these materials. In this context, friction-stir processing (FSP) could be very helpful to accomplish dissimilar joining and nanocomposite fabrication, simultaneously. This FSP technology was broadly employed to process polymer-matrix nanocomposites [46, 53–57] as well as the metal-matrix

nanocomposites [34, 37, 39, 40]. Meanwhile, there is not any report in the literature on dissimilar nanocomposite joining between aluminum and polymer by using friction-stirring. Thus, this idea is very interesting for future works to use from the mentioned nanocomposite joining concept to develop the dissimilar weldments between aluminum and polymer counterparts. Joining design, approach for introducing the secondary phase reinforcing agents, type of reinforcements, and their volume fractions can be considered as the variable of this new FSP concept further than the usual parameters of FSW

**Fig. 35** High magnification and high resolution TEM images from the aluminum-polymer interface for AA5059-HDPE dissimilar weldment [58]

technology. By optimizing these processing parameters, it is possible to control the quality and performance of dissimilar nanocomposite weldments.

3 Correlation between the microstructural features, mechanical property, and fracture behavior

Table 5 provides the summary from literature for main microstructural and mechanical characteristics of various processed dissimilar weldments. As can be found, depending on the type of aluminum alloy and polymer compound, different mechanical performances were noted for dissimilar joints in correlation with the microstructural details through the weld nugget. It is completely obvious that the low joining efficiency could be considered as the big challenge of dissimilar friction-stir weldments between aluminum and polymer. In the best condition, a strength ratio in the range of 60–70% as compared to the polymer substrate was reported, that is not still satisfactory for mechanical loading service condition. As described before, this drawback is attributed to large dissimilarity between these materials in terms of chemistry, physical, and mechanical property which can significantly affect the dissimilar material flow, inter-mixing, and subsequent physical and chemical interactions for formation of primary and secondary bonding. Another highlight point in Table 5 is relating to the fracture location. For all dissimilar weldments, fracture place was reported from the interface between aluminum and weld nugget due to feeble occurrence of chemical bonding at the interface. Also, the presence of solidification and flow defects in the weld nugget of dissimilar weldments as noted in Table 5 indicated very determinative in controlling the tensile flow property of joints. Contribution of some fraction of shrinkage micro-voids through the weld nugget is unavoidable caused by melting and solidification material during FSW process. However, the other defects in the case of processing materials and their dissimilarity in a joint design can be formed. Another important aspect of Table 5 is the joint design. Usually, better mechanical performance was reported for butt-joint design rather than lap-one, mainly due to intense materials intermixing and higher chance of mechanical interlocking and chemical interaction.

4 Metal-polymer interaction during FSW and formation of reaction layer at the interface

In the only reports by Khodabakhshi et al. [42, 58] on the characterization of interface and bonding mechanism between aluminum and polymer during dissimilar FSW joining, Bright Field-, Dark Field-Scanning (STEM), and High Resolution-

Transmission Electron Microscopy (HR-TEM), Energy-Dispersive X-ray Spectroscopy (EDS), and Fast Fourier Transform (FFT) diffraction analysis were implemented. Summary of the attained results is presented in Figs. 35, 36, and 37. The macro-, micro-, and nano-scale mechanical interlocking were defined as the main bonding mechanisms between aluminum fragments and melted/re-solidified polymer matrix by the formation of dissimilar weld nugget during FSW joining [58]. High-magnification STEM analysis from the Al-alloy fragments embedded in the polymer matrix in Fig. 35a–c revealed an ultrafine-grained structure with an average cell size of < 100 nm, suggesting that low-temperature severe plastic deformation (SPD) occurred during the FSW process. Furthermore, analysis of the Al-polymer interfaces in Figs. 36 and 37 revealed a 30-nm thick layer with a semi-crystalline aluminum structure elevated in levels of O and traces of C due to the solid-state chemical reactions. The main joining mechanisms are suggested to be the generation of nano-scale pores in a narrow region inside the metal surface oxide adjacent to the interface which accommodates infiltration of polymer, as well as secondary Vander-Waal's bonding. This bonding mechanism is a result of the interfacial chemical reactions, leading to significant improvements in the

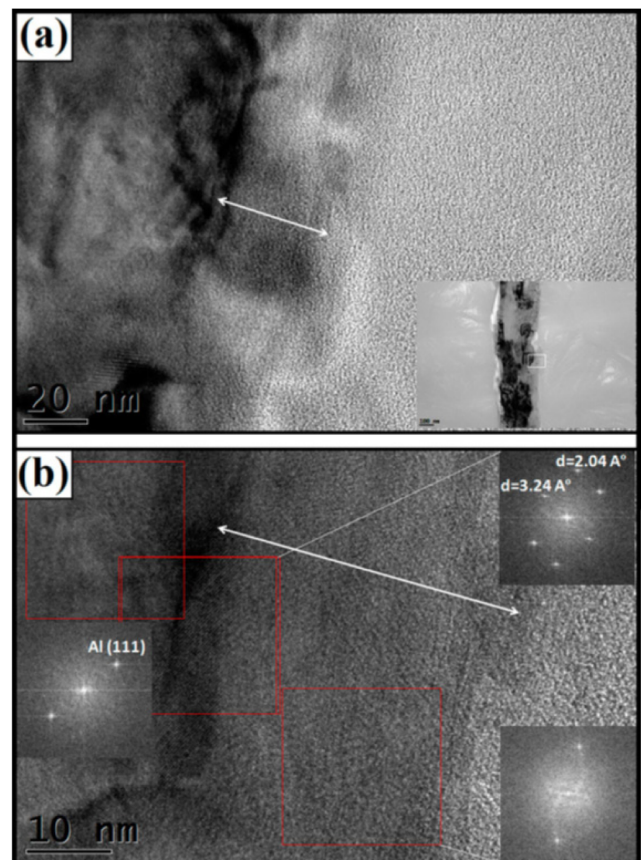


Fig. 36 (a) High magnification TEM image from the aluminum-polymer interface. (b) The related crystallographic orientation relationship at the interface [58]

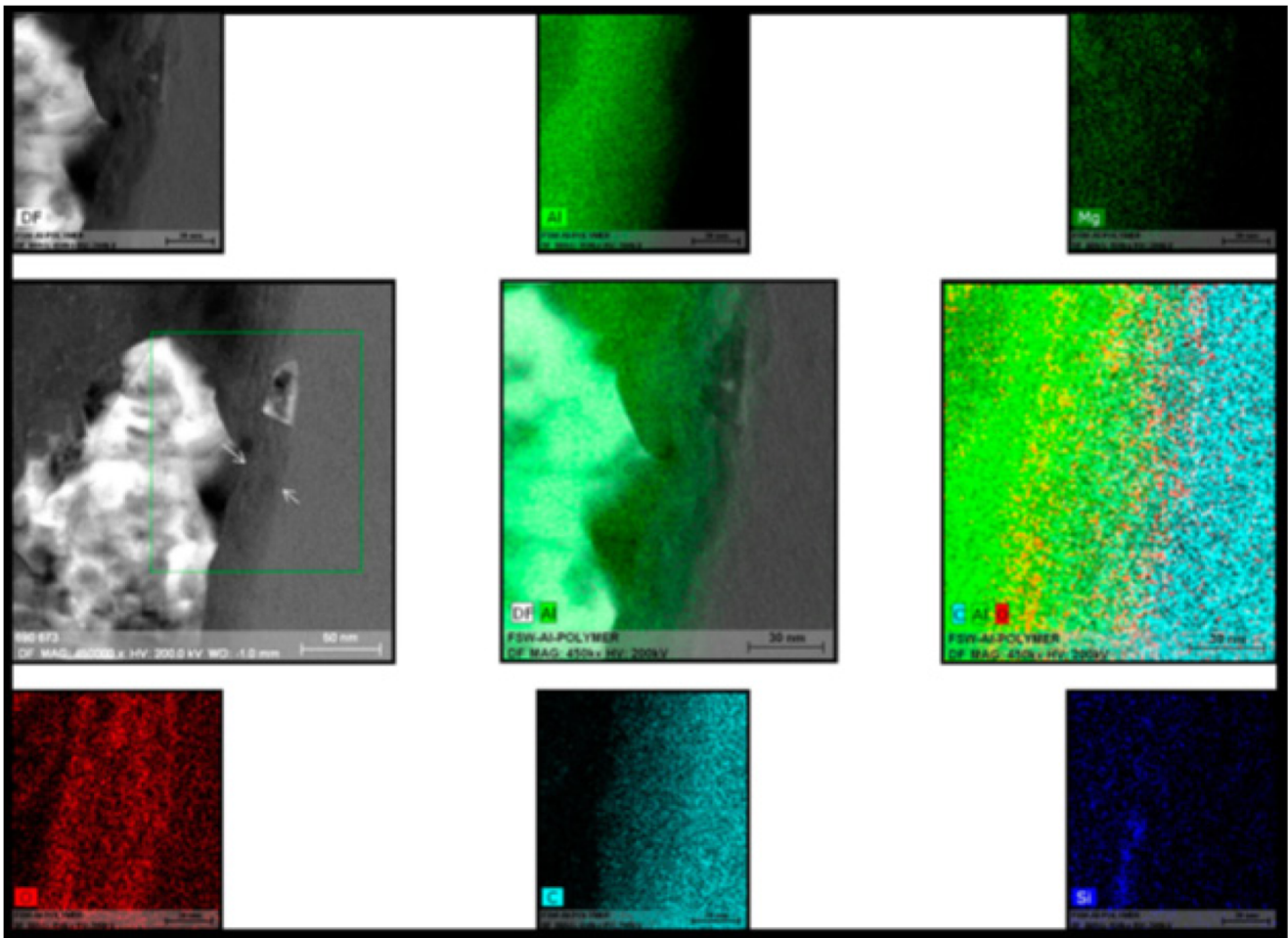


Fig. 37 The EDS STEM elemental mapping analysis results from the aluminum-polymer interface after FSW at high magnification [58]

mechanical properties of the joint as compared with the polymer substrate.

$$\rho \frac{\partial u_i \partial u_j}{\partial x_i} = -\frac{\partial P}{\partial x_j} + \frac{\partial}{\partial x_i} \left(\mu \frac{\partial u_i}{\partial x_j} + \mu \frac{\partial u_j}{\partial x_i} \right) - \rho U_1 \frac{\partial u_j}{\partial x_1} \quad (2)$$

$$\mu = \frac{\sigma_e}{3\dot{\epsilon}} = \frac{1}{3\alpha\dot{\epsilon}} \operatorname{arcsinh} \left(\frac{Z}{A} \right)^{\frac{1}{n}} = \frac{1}{3\alpha\dot{\epsilon}} \operatorname{arcsinh} \left(\frac{\dot{\epsilon} \exp \left(\frac{Q}{RT} \right)}{A} \right)^{\frac{1}{n}} \quad (3)$$

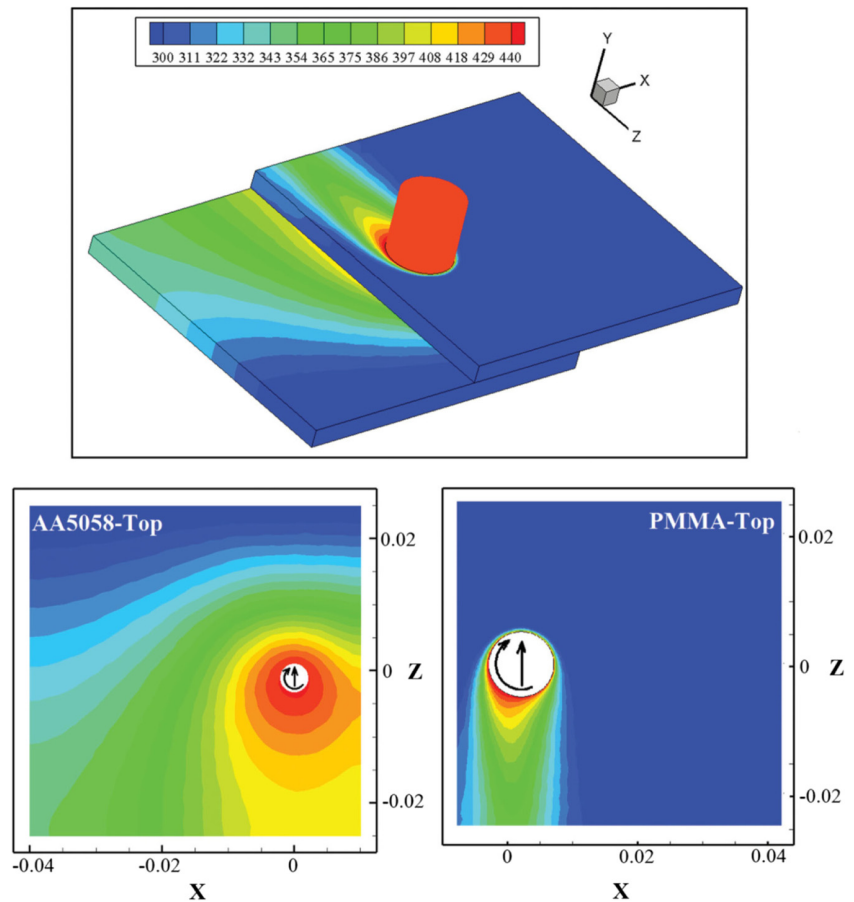
5 Thermo-mechanical modeling

As the same as similar and dissimilar FSW of metals and alloys, modeling and simulation based on thermo-mechanical concept is a valuable approach to predict the dissimilar mixing and joining of metals and polymers in terms of thermal data as well as the deformation flow profile. The only report in the simulation field was by Aghajani Derazkola et al. [51] on the dissimilar FSW lap-joining of AA5058 aluminum alloy and poly-methyl-methacrylate (PMMA) polymer, by combining the 3D non-linear heat transfer equation containing the internal heat source (Q_{total}), the momentum conservation principle, and Zener–Hollomon equation, as follows [43, 51]:

$$k \left(\frac{\partial^2 T}{\partial x^2} + \frac{\partial^2 T}{\partial y^2} + \frac{\partial^2 T}{\partial z^2} \right) + Q_{\text{Total}} = \rho c \frac{\partial T}{\partial t} \quad (1)$$

where T is the temperature profile, ρ is the density, c is the heat capacity, k is the thermal conductivity, u is the velocity vector, U_1 is the traversal velocity, P is the forging pressure during welding, μ is the non-Newtonian viscosity, σ_e is the flow stress, $\dot{\epsilon}$ is the strain rate, Z is the Zener–Hollomon parameter, Q is the activation energy, R is the universal gas constant, α , A , and n are the material constants [43]. For modeling, some assumptions were imposed on the solving the equations as compared to the real state, such as (i) non-Newtonian fluid flow behavior with visco-plastic trend, (ii) considering the materials flow and intermixing by Eulerian solution and adaptive meshing, (iii) not involving the crystal structure changing for polymer by melting during FSW process, and (iv)

Fig. 38 Thermo-mechanical modeling results for the temperature gradient within the aluminum alloy below sheet and PMMA top polymer sheet during FSW at a lap-joint design [51]



ignoring the liquid-state and solid-state chemical reactions between aluminum and polymer during mixing. For more information, refer to the work of Aghajani Derazkola et al. [51]. According to the attained temperature gradients presented in Fig. 38, the peak temperature at the weld nugget was monitored higher than the T_g point of PMMA and below than the melting point of the aluminum substrate around the softening region. Materials flow and inter-mixing during dissimilar joining of aluminum and polymer are compared based on the simulation and experimental results in Fig. 39. In this regard, more studies are required to accompany the modeling procedure more close to the experimental phenomenon. Since, as observed, the temperature in the stir zone is usually higher than the melting point of polymer and polymer during dissimilar joining is in the liquid state, meanwhile, aluminum is in the solid-state. Therefore, a combined computational fluid dynamic (CFD)/finite element (FE) model is required to consider both of two solid and liquid media beside of each other and their related interactions. It is a quite interesting idea to continue the research studies on the modeling and simulation of metal and polymer dissimilar friction-stir joining.

6 Possible potential areas, future directions, and observed gaps

The principle of metal/polymer FSW is to make hybrid structures where strength is provided from the metallic partner and lightweight is fulfilled from the polymeric side. This type of joining cannot be achieved through conventional fusion-based welding because of large dissimilarities between the physical properties of the metals and the polymers (i.e., melting temperature). Therefore, to reach this goal, solid-state welding operations, where none of the base materials is melted, shall be employed. It is worth mentioning that other joining operations like adhesive bonding may not possess the required strength. FSW gives substantial shearing stresses and blending activities, which actuates adequate warmth to join divergent materials (i.e., polymer and metal), where combination welding is incomprehensible. This can fulfill the ideal designation of auxiliary properties. However, as described in the present review, the current state of art needs more developments. A maximum dissimilar joint strength ratio of around 60% was reported during transverse tensile testing. Since for practical applications especially in the case of automotive industry, joint strength is a vital issue, therefore, the produced

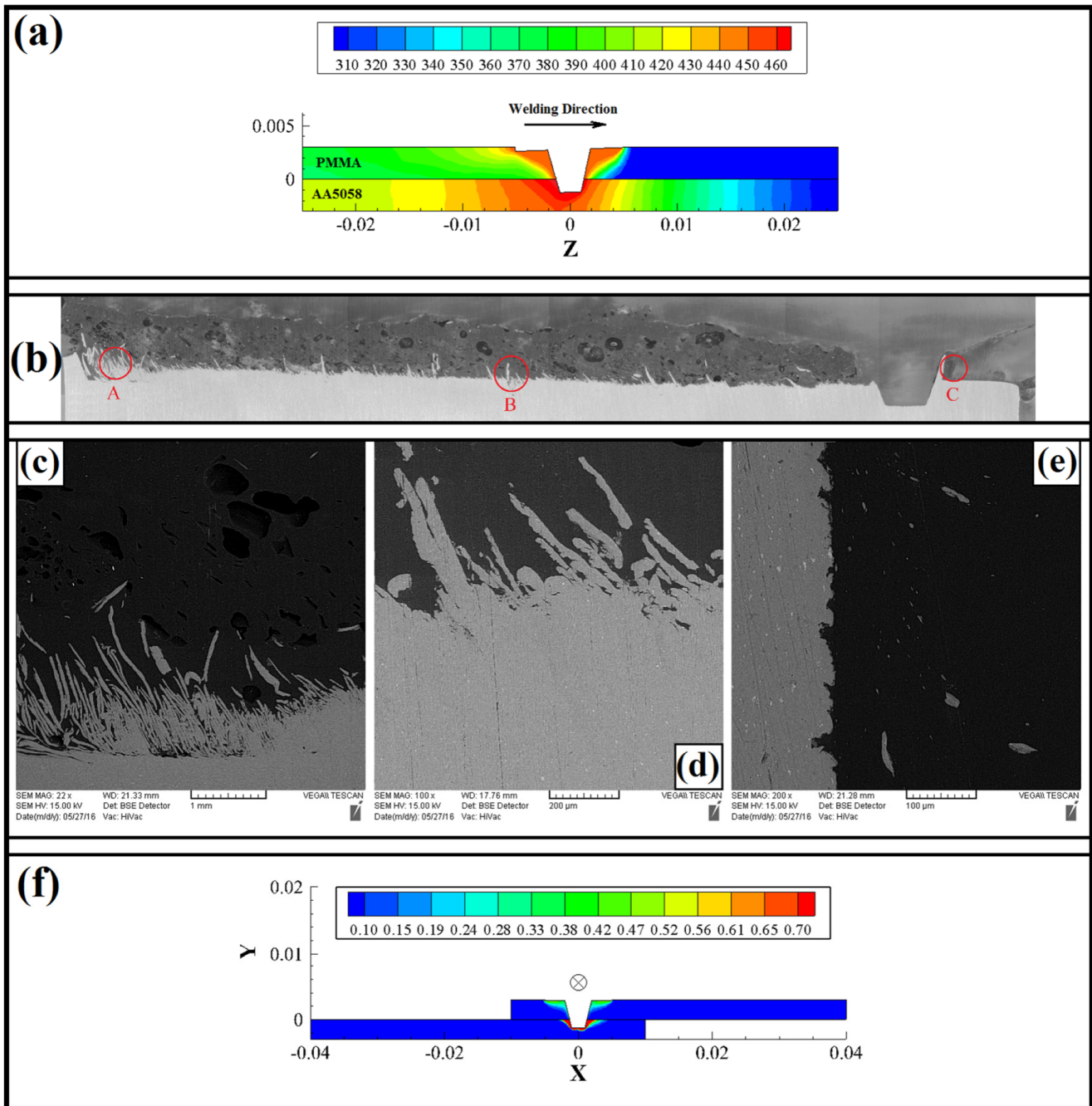


Fig. 39 (a) The simulation temperature results for the weld nugget cross section. (b–e) Experimental longitudinal and thickness cross-sectional profiles. (f) Material flow contours [51]

dissimilar metal-polymer weldments by FSW process up to now undoubtedly do not possess enough satisfaction for applying in service conditions under severe loading acts. As a main future prospect, improving the mechanical strength of metal-polymer dissimilar welds can be considered as an outlook, maybe by designing some new modifications on the FSW technology such as introducing the reinforcing ceramic nanoparticles into the weld nugget during dissimilar joining. Therefore, still the main challenge is improving the mechanical strength of dissimilar

friction-stir weldments between aluminum alloys and polymers for future studies, maybe by implantation of some innovations on design and processing.

7 Summary, concluding remarks, and outlook

In this critical review, potentials and capabilities of linear FSW process for solid-state dissimilar joining of metal-polymer bimetallic structures were illustrated and compared

in terms of joint quality, material mixing, flow pattern, soundness, microstructure, mechanical property, interfacial bonding, and thermo-mechanical modeling.

- According to the presented systematic results from the literature, formation of dissimilar weld nugget between metal and polymer and its geometry in terms of size and shape is very operative in the occurrence of dissimilar bonding, as it was found strongly depended on the type of metal and structure of the polymer.
- Toward reducing the physical and mechanical differences between metal and polymer couples by switching to soft metals such as aluminum and polymers with more complex structures (higher number and larger chains), the formation of a sound and defect-free weld was revealed probably in a wide range of processing parameters.
- Macro-, micro-, and nano-scale mechanical interlocking defined as the main bonding mechanisms aided by physical and chemical interaction according to the Van-der Waals effect and formation of a thin oxide layer at the interface.
- Herein, the contribution, importance, and impact of these bonding phenomena were significantly influenced by the processing parameters and especially tool design, rotational speed, traverse velocity, and tool tilting angle.
- With regard to the joint design, based on the current state of the art in the literature, butt-joint design displayed more effectiveness rather than the lap-one due to a higher chance for the formation of mechanical interlocks and larger surfaces for the physical and chemical interactions.
- A maximum dissimilar joining efficiency of ~60% was reported with failure location from the polymer side as the weakest base material.

References

1. Cho JH, Jae Kim W, Gil Lee C (2014) Texture and microstructure evolution and mechanical properties during friction stir welding of extruded aluminum billets. *Mater Sci Eng A* 597:314–323
2. Garcés JM, Moll DJ, Bicerano J, Fibiger R, McLeod DG (2000) Polymeric nanocomposites for automotive applications. *Adv Mater* 12(23):1835–1839
3. Oliveira PHF, Amancio-Filho ST, dos Santos JF, Hage E Jr (2010) Preliminary study on the feasibility of friction spot welding in PMMA. *Mater Lett* 64(19):2098–2101
4. Bilici MK, Yüklér Aİ, Kurtulmuş M (2011) The optimization of welding parameters for friction stir spot welding of high density polyethylene sheets. *Mater Des* 32(7):4074–4079
5. Cole GS, Sherman AM (1995) Light weight materials for automotive applications. *Mater Charact* 35(1):3–9
6. Amancio-Filho ST, dos Santos JF (2009) Joining of polymers and polymer–metal hybrid structures: recent developments and trends. *Polym Eng Sci* 49(8):1461–1476
7. David E, Lazar A (2003) Adhesive bonding between aluminium and polytetrafluoroethylene. *J Mater Process Technol* 143(144):191–194
8. Yusof F, Yukio M, Yoshiharu M, Abdul Shukor MH (2012) Effect of anodizing on pulsed Nd:YAG laser joining of polyethylene terephthalate (PET) and aluminium alloy (A5052). *Mater Des* 37:410–415
9. Grujicic M, Sellappan V, Omar MA, Seyr N, Obieglo A, Erdmann M, Holzleitner J (2008) An overview of the polymer-to-metal direct-adhesion hybrid technologies for load-bearing automotive components. *J Mater Process Technol* 197(1–3):363–373
10. Wahba M, Kawahito Y, Katayama S (2011) Laser direct joining of AZ91D thixomolded mg alloy and amorphous polyethylene terephthalate. *J Mater Process Technol* 211(6):1166–1174
11. Goushegir SM, dos Santos JF, Amancio-Filho ST (2014) Friction spot joining of aluminum AA2024/carbon-fiber reinforced poly(phenylene sulfide) composite single lap joints: microstructure and mechanical performance. *Mater Des* 54:196–206
12. Arici A, Sinmazçelyk T (2005) Effects of double passes of the tool on friction stir welding of polyethylene. *J Mater Sci* 40(12):3313–3316
13. Liu FC, Liao J, Nakata K (2014) Joining of metal to plastic using friction lap welding. *Mater Des* 54:236–244
14. Tres PA (2014) 5 - welding techniques for plastics. In: Tres PA (ed) *Designing plastic parts for assembly* (seventh edition). Hanser, pp 83–166
15. Jones I (2013) 10 - Laser welding of plastics*. In: Katayama S (ed) *Handbook of laser welding technologies*. Woodhead Publishing, pp 280–301e
16. Bergmann JP, Stambke M (2012) Potential of laser-manufactured polymer-metal hybrid joints. *Phys Procedia* 39:84–91
17. Berry DH, Namkanisorn A (2005) Fracture toughness of a Silane coupled polymer-metal Interface: Silane concentration effects. *J Adhes* 81(3–4):347–370
18. Matheny MP, Graff KF (2015) 11 - ultrasonic welding of metals. In: Gallego-Juárez JA, Graff KF (eds) *Power ultrasonics*. Woodhead Publishing, Oxford, pp 259–293
19. Yan P, Güngör ÖE, Thibaux P, Liebeherr M, Bhadeshia HKDH (2011) Tackling the toughness of steel pipes produced by high frequency induction welding and heat-treatment. *Mater Sci Eng A* 528(29–30):8492–8499
20. Abibe AB, Amancio-Filho ST, dos Santos JF, Hage E Jr (2013) Mechanical and failure behaviour of hybrid polymer–metal staked joints. *Mater Des* 46:338–347
21. Blaga L, Bancilă R, dos Santos JF, Amancio-Filho ST (2013) Friction riveting of glass–fibre-reinforced polyetherimide composite and titanium grade 2 hybrid joints. *Mater Des* 50:825–829
22. Balle F, Wagner G, Eifler D (2007) Ultrasonic spot welding of aluminum sheet/carbon fiber reinforced polymer – joints. *Mater Werkst* 38(11):934–938
23. Balle F, Wagner G, Eifler D (2009) Ultrasonic metal welding of Aluminium sheets to carbon fibre reinforced thermoplastic composites. *Adv Eng Mater* 11(1–2):35–39
24. Balle F, Eifler D (2012) Statistical test planning for ultrasonic welding of dissimilar materials using the example of aluminum-carbon fiber reinforced polymers (CFRP) joints, *Statistische Versuchsplanung zum Ultraschallschweißen artfremder Werkstoffe am Beispiel von Aluminium-Kohlefaser-Kunststoff-Verbunden (CFK)*. *Mater Werkst* 43(4):286–292
25. Goushegir SM, dos Santos JF, Amancio-Filho ST (2015) Influence of process parameters on mechanical performance and bonding area of AA2024/carbon-fiber-reinforced poly(phenylene sulfide) friction spot single lap joints. *Mater Des* 83:431–442
26. Mitschang P, Velthuis R, Didi M (2013) Induction spot welding of metal/CFRPC hybrid joints. *Adv Eng Mater* 15(9):804–813

27. He X, Gu F, Ball A (2014) A review of numerical analysis of friction stir welding. *Prog Mater Sci* 65:1–66
28. Nandan R, DebRoy T, Bhadeshia HKDH (2008) Recent advances in friction-stir welding – process, weldment structure and properties. *Prog Mater Sci* 53(6):980–1023
29. Khodabakhshi F, Arab SM, Švec P, Gerlich AP (2017) Fabrication of a new Al-mg/graphene nanocomposite by multi-pass friction-stir processing: dispersion, microstructure, stability, and strengthening. *Mater Charact* 132:92–107
30. Mishra RS, Ma ZY (2005) Friction stir welding and processing. *Mater Sci Eng R* 50(1–2):1–78
31. Khodabakhshi F, Gerlich AP, Švec P (2017) Fabrication of a high strength ultra-fine grained Al-mg-SiC nanocomposite by multi-step friction-stir processing. *Mater Sci Eng A* 698:313–325
32. Khodabakhshi F, Gerlich AP (2018) Potentials and strategies of solid-state additive friction-stir manufacturing technology: a critical review. *J Manuf Process* 36:77–92
33. Simar A, Bréchet Y, de Meester B, Denquin A, Gallais C, Pardoen T (2012) Integrated modeling of friction stir welding of 6xxx series Al alloys: process, microstructure and properties. *Prog Mater Sci* 57(1):95–183
34. Khodabakhshi F, Gerlich AP, Švec P (2017) Reactive friction-stir processing of an Al-Mg alloy with introducing multi-walled carbon nano-tubes (MW-CNTs): microstructural characteristics and mechanical properties. *Mater Charact* 131:359–373
35. Rafiei R, Moghaddam AO, Hatami M, Khodabakhshi F, Abdolazadeh A, Shokuhfar A (2017) Microstructural characteristics and mechanical properties of the dissimilar friction-stir butt welds between an Al-mg alloy and A316L stainless steel. *Int J Adv Manuf Technol* 90(9–12):2785–2801
36. Rafiei R, Shamanian M, Fathi MH, Khodabakhshi F (2018) Dissimilar friction-stir lap-welding of aluminum-magnesium (AA5052) and aluminum-copper (AA2024) alloys: microstructural evolution and mechanical properties. *Int J Adv Manuf Technol* 94(9):3713–3730
37. Khodabakhshi F, Ghasemi Yazdabadi H, Kokabi AH, Simchi A (2013) Friction stir welding of a P/M Al–Al₂O₃ nanocomposite: microstructure and mechanical properties. *Mater Sci Eng A* 585:222–232
38. Khodabakhshi F, Marzbanrad B, Shah L, Jahed H, Gerlich A (2017) Friction-stir processing of a cold sprayed AA7075 coating layer on the AZ31B substrate: structural homogeneity, microstructures and hardness. *Surf Coat Technol* 331:116–128
39. Khodabakhshi F, Simchi A, Kokabi AH, Gerlich AP (2016) Similar and dissimilar friction-stir welding of an PM aluminum-matrix hybrid nanocomposite and commercial pure aluminum: microstructure and mechanical properties. *Mater Sci Eng A* 666:225–237
40. Khodabakhshi F, Simchi A, Kokabi AH, Gerlich AP, Nosko M, Švec P (2017) Influence of hard inclusions on microstructural characteristics and textural components during dissimilar friction-stir welding of an PM Al–Al₂O₃–SiC hybrid nanocomposite with AA1050 alloy. *Sci Technol Weld Join* 22(5):412–427
41. Ratanathavorn W, Melander A (2015) Dissimilar joining between aluminium alloy (AA 6111) and thermoplastics using friction stir welding. *Sci Technol Weld Join* 20(3):222–228
42. Khodabakhshi F, Haghshenas M, Sahraeinejad S, Chen J, Shalchi B, Li J, Gerlich AP (2014) Microstructure-property characterization of a friction-stir welded joint between AA5059 aluminum alloy and high density polyethylene. *Mater Charact* 98:73–82
43. Aghajani Derazkola H, Khodabakhshi F (2019) Intermetallic compounds (IMCs) formation during dissimilar friction-stir welding of AA5005 aluminum alloy to St-52 steel: numerical modeling and experimental study. *Int J Adv Manuf Technol* 100:2401–2422
44. Derazkola HA, Elyasi M (2018) The influence of process parameters in friction stir welding of Al-mg alloy and polycarbonate. *J Manuf Process* 35:88–98
45. Huang Y, Meng X, Wang Y, Xie Y, Zhou L (2018) Joining of aluminum alloy and polymer via friction stir lap welding. *J Mater Process Technol* 257:148–154
46. Huang Y, Meng X, Xie Y, Wan L, Lv Z, Cao J, Feng J (2018) Friction stir welding/processing of polymers and polymer matrix composites. *Compos Part A* 105:235–257
47. Moshwan R, Rahmat SM, Yusof F, Hassan MA, Hamdi M, Fadzil M (2014) Dissimilar friction stir welding between polycarbonate and AA 7075 aluminum alloy. *Int J Mater Res* 106(3):258–266
48. Patel AR, Dalwadi CG, Rana HG (2016) A review: dissimilar material joining of metal to polymer using friction stir welding (FSW), IJSTE. *Int J Sci Tech Eng* 2(10):702–706
49. Rahmat SM, Hamdi M, Yusof F, Moshwan R (2014) Preliminary study on the feasibility of friction stir welding in 7075 aluminium alloy and polycarbonate sheet. *Mater Res Innov* 18(sup6):S6–515-S6-519
50. Derazkola HA, Kashiry Fard R, Khodabakhshi F (2018) Effects of processing parameters on the characteristics of dissimilar friction-stir-welded joints between AA5058 aluminum alloy and PMMA polymer. *Weld World* 62(1):117–130
51. Derazkola HA, Khodabakhshi F, Simchi A (2018) Friction-stir lap-joining of aluminium-magnesium/poly-methyl-methacrylate hybrid structures: thermo-mechanical modelling and experimental feasibility study. *Sci Technol Weld Join* 23(1):35–49
52. Shahmiri H, Movahedi M, Kokabi AH (2017) Friction stir lap joining of aluminium alloy to polypropylene sheets. *Sci Technol Weld Join* 22(2):120–126
53. H.C M, Kailas SV (2018) Fabrication of localised aluminium foam by a novel polymeric blowing agent. *Mater Charact* 142:340–351
54. Aghajani Derazkola H, Simchi A (2018) Effects of alumina nanoparticles on the microstructure, strength and wear resistance of poly(methyl methacrylate)-based nanocomposites prepared by friction stir processing. *J Mech Behav Biomed Mater* 79:246–253
55. Ali AA, El-Meniawi MAH, Khafagi SM (2015) A novel Bi-processing technique for metal matrix nanocomposites. *Int J Adv Manuf Technol* 78(5):907–915
56. Barmouz M, Shahi P, Asadi P (2014) 14 - friction stir welding/processing of polymeric materials. In: Givi MKB, Asadi P (eds) *Advances in friction-stir welding and processing*. Woodhead Publishing, pp 601–670
57. Okada T, Uchida S, Nakata K (2014) Direct joining of aluminum alloy and plastic sheets by friction lap processing. *Mater Sci Forum* 794-796:395–400
58. Khodabakhshi F, Haghshenas M, Chen J, Shalchi Amirkhiz B, Li J, Gerlich AP (2017) Bonding mechanism and interface characterization during dissimilar friction stir welding of an aluminium/polymer bi-material joint. *Sci Technol Weld Join* 22(3):182–190

Publisher's note Springer Nature remains neutral with regard to jurisdictional claims in published maps and institutional affiliations.